공학박사학위논문

민감도 기반 위상최적화 알고리즘을 이용한 텍스쳐 합성 및 패턴 이미지 생성에 관한 연구

Texture Synthesis and Pattern Image Generation by Sensitivity-based Topology Optimization

2019년 8월

서울대학교 대학원

기계항공공학부

김 은 일

민감도 기반 위상최적화 알고리즘을 이용한 텍스쳐 합성 및 패턴 이미지 생성에 관한 연구

Texture Synthesis and Pattern Image Generation by Sensitivity-based Topology Optimization

지도교수 김 윤 영

이 논문을 공학박사 학위논문으로 제출함

2019 년 4 월

서울대학교 대학원

기계항공공학부

김 은 일

김은일의 공학박사 학위논문을 인준함

2019 년 6 월

위 원 장 : 조 맹 효

부위원장 : 김 윤 영

위 원 : 윤 병 동

위 원 : 김 도 년

위 원 : 이 중 석

ABSTRACT

Texture Synthesis and Pattern Image Generation by Sensitivity-based Topology Optimization

Eunil Kim
School of Mechanical and Aerospace Engineering
The Graduate School
Seoul National University

Texture and pattern are graphic images composed of repetitive contents. Images can be generated in a variety of ways depending on motifs which are repeated contents and how they are arranged. In this thesis, we propose a method to synthesize unique and various texture and pattern images from a small source image(motif) by using sensitivity-based topology optimization algorithm for heat transfer system. In the process of generating textures or patterns, it is most important that the small images which make up large images such as textures and patterns should be naturally and seamlessly connected. In this study, we present two methods for this. As the first method, a patch-based texture synthesis in computer vision is introduced to produce images with repeated content but less regularity. In texture synthesis, patches with

similar contents are copied from the source image and stitched so that they are connected naturally. Because selected patches are slightly different but have similar content, so the synthesized image is a texture or a semi-regular pattern. To connect the patches naturally, finding the stitching seam(path) is most important. For that, sensitivity-based topology optimization for the heat transfer system was employed instead of algorithms previously used in computer vision. In particular, a two-loop algorithm has been devised that includes updating of key parameters for convergence to a single path that is not often considered in conventional topology optimization. After verifying the proposed method through simple benchmark-type problems, several texture synthesis examples are considered and the convergence behavior and iteration history of the optimization algorithm are also investigated. A series of successfully solved numerical examples by the developed method indicates that it is an effective alternative method for texture synthesis. Another method to generate repetitive images is to simultaneously consider the connectivity between motifs to be repeated for a pattern while creating them. The motifs designed in this way are connected seamlessly at the boundary line, and constitute a pattern image in which the motifs are regularly arranged. In addition, different kinds of patterns can be synthesized depending on the manner in which motifs are repeated. We have actually applied the patterns created by the proposed method to several products that are easily accessible in everyday life. We have successfully generated regular patterns and semi-regular textures using a sensitivity - based topology optimization algorithm

in different ways, and it is found that the proposed method can be a new way of generating repetitive images such as textures and patterns.

Keywords: Texture synthesis, Pattern generation, Gradient-based algorithm, Topology optimization, Heat transfer

Student Number: 2013-30193

CONTENTS

LIST OF TABLES

LIST OF FIGURES

CHAPTER 1
INTRODUCTION

1.1 Motivation

A pattern is an image of arrangement or shape that is repeated regularly. A repeating unit image in a pattern is called a motif. Patterns are used in many areas of our lives, from fashion to interior design and computer graphics. Patterns with repetitive content give a sense of stability and are effective in expressing a specific theme, including symbols or logos. This is one of the reasons why pattern images are widely used in popular world-class goods. On the other hand, the pattern may feel monotonous because its motifs are uniformly arranged. But pattern images can be made more interesting using unique and creative motifs. An automatic computer design algorithm has already been developed to produce unique images, but this was for stand-alone images, not for original pattern images. In order to form a pattern

from a motif, motifs must be seamlessly connected at the boundary. Therefore, in order to create a unique and long-lasting pattern, it is necessary to consider the connectivity when motifs are repeatedly connected in the process of generating motifs by automatic image design algorithm.

Texture synthesis is the process of creating a large image that retains similar content from a small source image. This is a widely used technology in the field of computer vision and is a fundamental research field. As mentioned earlier, a pattern is an image in which the same motif is repeatedly formed. If the motifs are not simply repeated and the similar parts are copied from the motifs through texture synthesis so that the connections are well connected, a semi-regular and attractive image can be obtained. Also, various textures can be created depending on the part to be connected in one motif.

From a single motif, both the pattern image, which is a regular image that maintains its characteristics, and the texture, which is a semi - regular image, can be combined to broaden the area of image composition and increase the effectiveness of motifs. Also, the main parts in the process of this are all by topology optimization algorithms for heat transfer phenomena.

1.2 Review of previous researches

Topology optimization is a design method that finds the optimal material distribution by minimizing the given objective function while satisfying constraints [1]. It originated in the engineering design of structures [2] but has been expanded to most areas of engineering and science where the governing equations describing the physics of interest [3] are available containing even the synthesis of rigid-body mechanisms [4], acoustic system design [5, 6], metamaterial design [7, 8] and the structural design in a thermal system [9-11]. Studies on topology optimization have been conducted for the effective design of high-resolution structures for 3D printing [12, 13] as well as the simultaneous consideration of the performance and appearance of structures [14].

In a typical two-dimensional (2D) topology optimization setup, the design domain is discretized into fine elements, each of which is typically a rectangular continuum element occupying an area. To configure the topological layout of an optimal design, relative element density as a design variable is assigned to each finite element. It can continuously vary between zero and one, corresponding to a void and material state, respectively. The design variable is updated iteratively to improve the given objective function, which is typically compliance, while trying to satisfy constraint equations, as that relating to mass. Finally, a converged layout consisting of a distribution of design values of zero or one is obtained. To ensure the convergence

of the design variables, one may penalize the design-variable-dependent element stiffness [1].

Texture synthesis is the process of generating a larger image from a smaller source image while maintaining its original characteristics. The synthesis has been studied through various methods, including pixel-based methods [21, 22], patch-based methods [23-26], and texture optimization methods [27, 28]. In recent years, research using the convolutional neural networks has been also presented [29]. The authors presented a new method of texture synthesis that is based on convolutional neural networks and extracted statistics of pre-trained deep features. They extended this approach to the style transfer problem which is similar to texture synthesis and a traditional problem in computer vision [30]. After that, based on this method, research has been carried out considering the characteristics of structured texture by using correlations among deep features [31]. In some cases, the computation cost has been improved using feed-forward convolutional networks [32] and synthesis quality has improved by combining Markov random field with convolutional neural networks [33].

Pixel-based and patch-based methods are methods of copying and pasting the most similar parts of a neighboring area from a source image as pixel or patch units, and then gradually complete the result image. The patch-base method has two processes.

The first process in the path-based method is to select patches from a source image and arrange them to make them look similar to neighboring patches in the region of overlap between adjacent patches. The sum of squared differences (SSD) in the overlapping region is used as the measure of patch similarity. Patches that have the smallest SSD with neighboring patches are sequentially searched in the source image. The second process is to stitch the patches together along a seam to connect them naturally. In previous studies, dynamic programming [24] and graph cut [23] have been used to find seams for stitching patches.

The studies most directly related to this thesis, where the original problem has no direct physical principle, are on robot path planning [15] and aesthetic image generation [16]. However, to the best of the authors' knowledge, no study to date has employed topological optimization for natural-looking patch stitching. We deal with a simulated physical problem with inherited characteristics of texture synthesis, there is a major challenge in the topology optimization and a difference in setting up a computational model for topology optimization. Another remark to make regarding the present topology optimization formulation is that unlike most such optimizations using planar continuum elements, we use a ground structure model consisting of grid line elements surrounding pixels in the overlapping region. Although the patch information is based on the RGB values in each pixel (corresponding to each finite element of the continuum plane), the matching cost M is defined between two adjacent pixels in the overlapping region. Therefore, we assign the value of matching

cost to the grid line elements. Similar ground structure models have been used to solve structural problems in trusses [17-19] and problems of linkage mechanism synthesis [4, 20], but no earlier effort has been made to make use of pixel-interfacing grid line elements for texture synthesis. A direct analogy between the optimal seam and the optimal heat path in certain heat transfer problems is another way to yield a natural patch connection, and we use this novel method to solve the problem by formulating a topology optimization-based algorithm in a simulated physical space of heat transfer. This optimization-based method is also efficient because a sensitivity-based optimizer can be used even if the problem is elaborately formulated.

Since computational algorithms for art or aesthetic design were suggested in the early 1960s, there has been a growing interest in utilizing them for non-engineering or scientific fields. As pioneers in computer and algorithmic art, Verostko [34] presented computer-assisted algorithmic drawing where pen strokes controlled by his own algorithm create artistic images. Cohen [35] developed a painting program ARRON for abstract and representational drawings. Nake [36] and his colleagues have also presented pioneering works in the field. Mandelbrot [37] reported fractal images that were generated by computer graphics and mathematical equations. Recently, McCormack [38], Sims [39], Heijer and Eiben [40] and Todd and Latham [41] used evolutionary algorithms for image generation. Besides evolutionary algorithms, several other approaches have been developed, such as the parametric

method [42] and algorithms to simulate fungal hyphae growth [43]. There were interesting studies related to even brush strokes [44-46]. In the literature described above, images are mostly generated by simulating biological or physical phenomena. Unlike the aforementioned approaches to simulate physical phenomena, an alternative method of image generation by using a topology design optimization, which is called 'Variational art' has been studied [47]. Randomly-generated multiple starting and ending points, regarded as "heat sources and sinks" in the topology optimization algorithm, were used for each of different colors. In theory, any physical system may be considered, but to faciltate the generation of diverse images, they come up with a virtual design problem for which the process of the topology optimziation can be intepreted in the context of painting. For a virtual problem, they are proposing a topology optimization problem to find an efficient two-dimensional heat dissipating structural layout. Interestingly, the following interpretation may be possible in this case; a brush stroke drawn on a canvas by an artist may be viewed as an optimal heat path connecting a heat source and a heat sink in a two-dimensional plate under a constraint imposed on the mass used to form the path. In solving the virtual problem, one can use multiple heat sources (starting points) and sinks (ending points) simultaneously. This interpretation and freedom to choose the numbers and strengths of starting and ending points allow us to produce non-trivial (non-straight, thickness-varying) multiple brushing strokes, forming various images. Because the employed thermal problem is artificial, one can also distribute the sources and sinks randomly for image diversification. Furthermore, one can also vary the value of the

mass constraint (interpreted as the amount of paints or inks) quite arbitrarily and even juxtapose multiple solutions (images) if they are properly colored.

1.3 Outline of thesis

In Chapter 2, the theoretical background for topology optimization of the heat transfer system for the path planning and texture synthesis in computer vision is provided. The details include the governing equation of the heat transfer system, the finite element analysis for the system and the formulation of topology optimization. In addition, the problem definition of texture synthesis and image stitching, the matching cost which is a measure of the similarity between neighboring pixels and the graph model to represent information of pixels in an image are introduced.

In Chapter 3, texture synthesis research by using topology optimization of the heat transfer system is introduced. Texture synthesis is the process of creating a large image from a small source image while maintaining its characteristics. In this study, a new algorithm using heat transfer topology optimization is used instead of conventional algorithms used in computer vision for texture synthesis. Of several method of texture synthesis in computer vision, we have adopted a patch-based approach that connects multiple patches which are from the source image. It is important to find the path that connects the patches in order to connect the patches naturally. We have newly formulated the patch stitching problem in the heat transfer system by using the analogy between the patch stitching problem in the computer vision field and the path optimization problem in the heat transfer system. Because a sensitivity-based optimizer is used in this research, the proposed method is efficient to solve the optimization problem. This method based on topology optimization of

the heat system is applied for the first time in computer vision problems. To verify this method, several examples of image stitching and texture synthesis by using general images and images made by VA as a source image are provided.

In Chapter 4, a research on generating pattern images by using a motif created through Variational Art (VA) is introduced. The VA algorithm produces a single image (motif) through a topology optimization technique based on heat transfer phenomena. These images made by using VA are meaningful by themselves like as artworks or paintings. Because simply arranging these images cannot be a pattern without considering the connectivity of images, the methods for generating the motif considering the connectivity between them depending on the way of repetitive arrangement are presented. By using different motifs, various pattern images are obtained. In addition, VA is an automatic algorithm for image generation and works under the virtual physical phenomenon, so it is possible to create a very wide variety of patterns in a short time by setting parameters of the algorithm randomly. These patterns can be analyzed and categorized according to the characteristics, can be applied to sample products. In fact, various prototypes as a part of the research project to develop and commercialize the VA algorithm are provided.

In Chapter 5, the concluding remarks on this thesis are summarized. We used topology optimization techniques for heat transfer phenomena in all processes from

texture synthesis to pattern generation. Through this study, we prove the feasibility and expansion of the proposed heat transfer topology optimization method.

CHAPTER 2
BACKGROUND RESEARCH

2.1 Path planning by topology optimization in heat transfer system

In both of path optimization researches for VA and texture synthesis mentioned in Section 1.3, topology optimization of the heat transfer system was applied. Heat path optimization has been attempted to be applied to a variety of fields beyond the thermal system. In previous study [15], heat path topology optimization was applied to the problem of a robot path planning through analogy between two problems. The two-dimensional heat conduction plate is a space where a mobile robot can move, while the insulation region on the conducting plate is an obstacle where the robot cannot pass. Heat sources and sinks are the starting and ending points of a robot. The

governing equation for the two-dimensional steady-state thermal conduction plate is expressed as

$$k\nabla^2\theta - h\theta + Q = 0 \tag{2.1}$$

The symbols k and h are the coefficients of thermal conductivity and convective heat transfer. Heat generation is denoted by Q. In the formulation of this problem the source is modeled by heat generation as a starting point of the robot, and the sink is modeled by heat convection as an end point. By the finite element method for the analysis of the heat transfer system modeled in this way, the following equation of the system matrix is obtained.

$$\mathbf{K}\boldsymbol{\theta} = \mathbf{F} \tag{2.2}$$

where $\mathbf{K}$, $\boldsymbol{\theta}$ and $\mathbf{F}$ denote the stiffness matrix, nodal temperature vector and the load vector. These system components are assembled by using element-level matrices($\mathbf{K}_e^d$, $\mathbf{K}_e^v$) and vectors($\boldsymbol{\theta}_e$, $\mathbf{F}_e$) as follows,

$$\mathbf{K} = \sum_{e=1}^{N} \mathbf{K}_e^d + \sum_{e=1}^{N} \mathbf{K}_e^v \tag{2.3}$$

$$\mathbf{F} = \sum_{e=1}^{N} \mathbf{F}_e \tag{2.4}$$

$$\boldsymbol{\theta} = \sum_{e=1}^{N} \boldsymbol{\theta}_e \tag{2.5}$$

where $\mathbf{K}_e^d$ and $\mathbf{K}_e^v$ are the element conduction matrix and the element convection matrix, $\mathbf{F}_e$ and $\boldsymbol{\theta}_e$ are the element force vector and the element temperature vector, respectively. For the topology optimization formulation, the thermal conductivity k_e of an element is interpolated with the following polynomial function

$$k_e = k_0 \rho_e^p \tag{2.6}$$

The robot path finding problem is dealt with as the problem of finding the most efficient heat path connecting the source and sink on the heat conducting plate. The objective function for topology optimization is to minimize the thermal compliance of the heat transfer system subject to the mass constraint of the heat path as

$$\underset{(\rho_1,\rho_2,\rho_3,\cdots,\rho_e)}{\text{minimize}} \ \Pi = \boldsymbol{\theta}^T \mathbf{K} \boldsymbol{\theta} \tag{2.7}$$

$$\text{subject to} \ \sum_{e=1}^{Ne} \rho_e V_e - M_0 \le 0 \tag{2.8}$$

where ρ_e , V_e and M_0 are the design variable, the element volume and allowable mass. However, since the mass(length) of the heat path cannot be predicted in advance, it is very difficult to choose a proper value of M_0 for the constraint condition. This issue remains in the problem of the path finding for texture synthesis as described in Chapter 3. In the study of [15], to set the proper constraint condition, the upper bound of mass M_0 is set to be continuously reduced according to the iteration number, but the minimum value $M_{\min}$ to be the straight distance between the heat source and the sink.

$$M_0(n) = \max(\aleph(n), M_{\min}) \tag{2.9}$$

$$\aleph(n) = \frac{\sum_{e=1}^{N} V_e}{n^2} \tag{2.10}$$

To solve this problem, a continuation method was applied, which varies the penalty exponent value of p in the polynomial interpolation function in the material interpolation. Various numerical examples of the path planning for avoiding obstacles with/without a stopover and for a real terrain were presented in [15]. This research was the first attempt to apply the sensitivity-based topology optimization algorithm to robot path planning.

2.2 Texture synthesis in computer vision

Texture synthesis problems in computer vision have been solved by different approaches. Our method is based on the patch-based method for texture synthesis. This arranges patches from a source image with similar characteristics in overlap regions and cuts them appropriately so that they look naturally continuous along their boundaries inside the regions. Specifically, patches with the smallest SSD in the overlap region are sequentially obtained from candidate patches of the source image. Then, using dynamic programming or the graph cut algorithm, seams that connect the patches naturally in the overlap regions are found. Figure 2 illustrates how patches are attached along the stitching line in the overlap region represented in gray when there is only one overlap region.

In the process of finding the optimal seam, Kwatra et al. [23] defined and made use of the matching cost M :

$$M(s,t,\mathbf{A},\mathbf{B}) = \frac{\left\|\mathbf{A}(s)-\mathbf{B}(s)\right\|+\left\|\mathbf{A}(t)-\mathbf{B}(t)\right\|}{\left\|G_{\mathbf{A}}^{d}(s)\right\|+\left\|G_{\mathbf{A}}^{d}(t)\right\|+\left\|G_{\mathbf{B}}^{d}(s)\right\|+\left\|G_{\mathbf{B}}^{d}(t)\right\|} \tag{2.4}$$

where $\mathbf{A}(s)$ and $\mathbf{B}(s)$ denote the RGB values of patches A and B at pixel s.

Symbol G_A^d (G_B^d) denotes the gradient of the pixel in patch A (B) along direction d, either horizontal or vertical. The matching cost $M(s,t,\mathbf{A},\mathbf{B})$ assigned to each edge of two interfacing pixels s and t of patches A and B is the sum of the differences of the RGB values of these pixels in each patch. Therefore, the smaller the matching cost, the smaller the difference between the adjacent pixels, and the patches can be naturally connected at the boundaries of the pixels. The optimal seam is found as one that minimizes the overall matching cost. A graph cut algorithm was used to this end by Kwatra et al. [23]. A graph model defined over the overlap region, covering pixels P1 to P9, is shown in the middle of Figure 2.2. We explain this model in some detail as we also use cost *M* in our formulation in Chapter 3. In the graph model, each pixel is represented as a node, and the matching cost of two adjacent pixels is assigned to the edge connecting the nodes. If a graph cut algorithm is applied, one can find a stitching seam plotted by the red line, and this has the minimum matching cost.

Figure 2.1 Stitching of two patches (left). The region of overlap of two patches is in gray (middle), and two patches are attached along the stitching line in the overlap area (right).

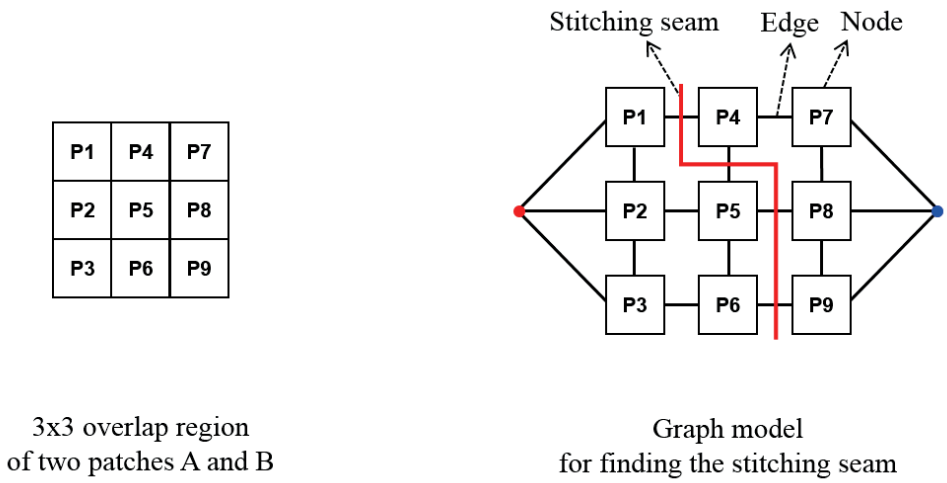

Figure 2.2 The overlap region of 3×3 pixels (left), the graph model of the overlap region consisting of nodes and edges for finding the stitching seam (middle).

CHAPTER 3
PATCH-BASED TEXTURE SYNTHESIS BY TOPOLOGY OPTIMIZATION METHOD

3.1 Overview

Texture synthesis is a fundamental problem in computer vision that has been studied in a variety of ways. The patch-based method of stitching multiple patches to produce a larger image is among the basic methods, and concerns this study as well. To stitch images for texture synthesis, the patch connection should be as natural as possible, although it is difficult to precisely define how "natural" it is. In this chapter, we propose a technique for texture synthesis that uses topology optimization where the natural connection is defined in the context of heat transfer. Conventional seam-finding methods typically use the graph cut algorithm inspired by fluid flow. On the other hand, we argue that an optimal seam is analogous to an optimal heat path

connecting a sink and a source, and find this path by solving an elaborate problem of topology optimization in a simulated physical space for heat transfer. Because the seam is the optimal heat path in the physical space, the naturalness of patch connection is directly acquired from the simulated physics. The optimal heat path is determined as a path that minimizes thermal compliance under some conditions. Because topology optimization is used, the procedure to find the optimal seam can be quite efficient due to the use of a sensitivity-based gradient optimizer.

Figure 3.1 shows the problem definition and an overview of the proposed seam-finding algorithm using the novel topology optimization method. The region of overlap of Patches A and B, in which an optimal seam is to be drawn, is discretized by finite elements (in this case, a set of finite grid lines). The optimal seam is then found as an optimal heat path connecting a heat source on top of the overlap region to a heat sink at its bottom under elaborately selected objective and constraint functions. The developed topology optimization-based method is discussed in details below. The iteration history in Figure 3.1 suggests that one of the main challenges in formulating the topology optimization in the simulated physical space is to ensure a single seam line (or single heat path line) while the seam makes the patch connection as natural as possible. Note that the issue of the formation of the single line does not appear in most physical problems in practice so that a special method must be devised to resolve the issue. Therefore, the objective function of the optimization (minimization) problem is chosen as the total mass of the heat path (corresponding

to the total length of the optimal seam line), weighted with matching cost M denoting the sum of differences of the RGB values in these pixels between patches in the overlap region [23]. Thermal compliance is treated as a constraint, where its upper bound is updated iteratively during optimization iterations. A unique, double-loop optimization technique that has not been used in typical topology optimization in real physical problems is developed in this study. The main contributions of our work can be summarized as follows:

1) We solve the texture synthesis problem in computer vision as a topology optimization problem in a simulated physical space in which the naturalness of patch connection is acquired through the heat transfer phenomenon.
2) To ensure a single-line optimal seam, we develop a double-loop topology optimization algorithm that minimizes the length of the heat path (seam) with updated constraints on thermal compliance.
3) Our method was validated using a set of problems and its effectiveness was demonstrated through application to various practical stitching problems.

3.2 Problem setup

3.2.1 Analogy

In the heat transfer phenomenon, heat is always flowing directionally from a heat source to a heat sink without discontinuity on the path. This is a unique feature that can be found in any heat transfer system that differs from those seen in the structure or other systems. In this study, we try to solve the texture synthesis problem by bringing the mathematical model of computer vision into the physical space of the natural phenomenon and applying the physical principle of heat transfer phenomenon to that problem. Because differentiable formulations are possible in a modeling based on a physical phenomenon, the design sensitivity information can be utilized. The problem of finding the seams in the overlap regions of patches using the graph model is very similar to that of finding the path of heat transfer in a grid structure model consisting of one-dimensional heat conductive elements. Table 3.1 compares the similarities of these two problems.

By the phenomenon of heat conduction taking place in a conducting plate, a heat source is connected by the shortest heat path to a heat sink, where the path is affected by the number of its segments (grid element). Here, conductivity is assumed to be constant everywhere. The illustration to the right in Figure 3.2 shows the grid structure model used to find the optimal heat path from a heat source to a heat sink located outside the overlap region. Since the elements constituting the grid structure

model are conceptually arranged at the boundaries of all the pixels in the overlap regions between the patches, the optimal heat path is intuitively identical to the seam for image stitching itself in the grid structure unlike in the graph model. In the case of the grid structure model, each pixel is defined by four nodes and surrounded by four heat conductive line (or 1D) elements. These notations are commonly used in finite element analysis, which we use to solve for heat conduction here. Figure 3.3 shows how the grid structure model in the right side of Figure 3.2 is modeled by an equivalent finite element model. The 1D heat conductive elements are denoted by numbers from 1 to 24 while the nodes are denoted by circled numbers from 1 to 16. It is assumed that all heat conductive elements have the same heat conduction coefficient of k=1 (properly non-dimensionalized) and the same length. With this model, the value of cost M is mapped to the volume of the 1D heat conductive element. In Figure 3.4, for example, the cost $M\left(\mathrm{P1},\mathrm{P4},\mathbf{A},\mathbf{B}\right)$ between pixels P1 and P4 in the graph model may correspond to the volume of element 16 connecting nodes 2 and 6, which determine the interface between pixels P1 and P4 in the grid structure model. We say $M\left(\mathrm{P1},\mathrm{P4},\mathbf{A},\mathbf{B}\right)=M_{16}$, where $\mathbf{A}$ and $\mathbf{B}$ are omitted without loss of generality. Note that in the finite element model, the heat source (input) and sink (output), denoted by S_i and S_o, respectively, are connected to nodes facing them as shown in Figure 3.3. Note that in this model, the two patches are assumed to be horizontally stitched. If they are vertically stitched, for instance, S_i and S_o should be located on the left and right sides of the overlap region.

3.2.2 Definition of weighted mass

To form a natural-looking seam with the finite element model shown on the right side of Figure 3.3, a topology optimization problem is set-up in the simulated physical space of heat transfer. To analyze this heat transfer model, we consider only steady-state thermal conduction without thermal convection. It is also assumed that the heat flows in only one way in each element of the grid structure. The governing equation for this heat transfer system can be written as [47]:

$$k\nabla^2 T + Q = 0 \tag{3.1}$$

where k is the thermal conductivity coefficient, T is temperature, and Q is the heat generated. Because the upper and lower boundaries of the overlap region are connected to a heat sink and a heat source, heat transfer from and to the overlap region takes place under boundary conditions. The heat flux, i.e., heat flow per unit area q, for each heat conduction element is calculated as

$$q = -k\nabla T \tag{3.2}$$

Heat flux is the quantity used to determine natural-looking seams through the minimization of the so-called thermal compliance. More details are provided in the next section. While a natural-looking seam may be effectively found through topology optimization of thermal compliance minimization, there is no guarantee that the path is a single-line path. To ensure this, we minimize the mass $\mathcal{M}$ of the total path that can be calculated as

$$\mathcal{M} = \sum_{e=1}^{N_e} \rho_e v_e \tag{3.3}$$

where the volume of the element v_e can be taken to be unity ($v_e = v_0 = 1$), and N_e is the total number of the heat conduction elements. Each element has a relative density variable ρ_e ($0 \le \rho_e \le 1$) that serves as the design variable of the optimization problem. To reflect the effect of matching cost, we use the weighted mass defined as

$$\mathcal{M} = \sum_{e=1}^{N_e} \rho_e v_e W_e = v_0 \sum_{e=1}^{N_e} \rho_e W_e \tag{3.4}$$

Weight W_e is defined as

$$W_e = \left(M_e \right)^r \tag{3.5}$$

where r is the parameter to improve convergence. We used $r = 2$ after some numerical tests. Because of the weighting factor W_e, a heat conduction element with a large matching cost was designated as less preferable in forming the path during mass minimization.

While both mass and thermal compliance should be simultaneously minimized, it is difficult to determine how much of each objective should contribute to form the objective function. Furthermore, it is not possible to find the theoretical condition for a single-line path. Therefore, we develop a double-loop topology optimization algorithm that is provided in Section 3.3.2.

3.2.3 Concept of path finding for patch stitching

To give an overview of the process of topology optimization in the simulated space of heat transfer, a toy problem of stitching simple two patches as illustrated in Figure 3.5. The overlap region of two patches is 3x3 pixels and they have obviously different two areas, dark and light. The overlap area is modeled as a grid structure and the matching cost is given to each element as shown in Figure 3.6. The path that

minimizes the sum of the values M_e becomes the stitching line. We can find that the obvious seam is the path passing through nodes 2, 6, 7, 11, and 15. Note that we intentionally assign a large value of $M_{\max}$ to the outmost elements of the grid structure to form a seam only inside the overlap region.

The process of topology optimization for the toy problem in Figure 3.6 is shown in Figure 3.7. In the double-loop topology optimization algorithm, a single objective function $\mathcal{M}$ with a loop-wise changing constraint on thermal compliance is used. The optimal seam is found after 26 iterations for the problem in Figure 5. The value of the objective function tends to decrease except near the ends of the iterations, and all ρ_e's at convergence reach either zero or one. If ρ_e is one, the grid element is considered part of the seam, and ρ_e becomes zero, and is not considered part of the seam. Our formulation should also ensure the disappearance of intermediate density elements, but this problem has been resolved in design problems [1]. The initial design variable was chosen to be 0.5, a neutral value. To observe convergence behavior, we may trace the value of the ρ_5 of the element connecting nodes 6 and 7 during the topology optimization iterations, as shown along the right sides of Figure 3.7. Although the problem considered is trivial, it shows that the proposed algorithm leads to the correct seam forming a single-line path at convergence. With this overview of the algorithm, we present its details in the next section.

3.3 Topology optimization formulation for patch stitching

In this section, we describe the proposed double-loop topology optimization algorithm performed in the simulated physical space of heat transfer. We begin with a single-loop topology optimization algorithm used as a building block for our method, which ensures single-line, natural-looking paths.

3.3.1 Matching cost-weighted mass minimization with thermal compliance constraint

To implement topology optimization, the overlap region is discretized into N_e finite grid elements, as illustrated in Figure 3.6, with a heat source on one side of the region and a heat sink on the other. The strengths of the source and sink are simply taken to be unity. The region, also referred to as the design domain in the standard terminology of topology optimization, is discretized by the finite elements. The procedure to form element ($\mathbf{K}_e$) and the global ($\mathbf{K}$) stiffness matrices is well known [48, 49]. Thus, we simply write the finite element equation:

$$\mathbf{K}\boldsymbol{\theta} = \mathbf{F} \tag{3.6}$$

where $\mathbf{F}$ denotes the external force vector reflecting the contributions of the heat sink and source while Q in Equation (3.1) is zero. The symbol $\boldsymbol{\theta}$ represents the

global nodal temperature vector. We use two-node 1D heat conduction elements. While in most typical topology optimization problems involving compliance, system compliance is minimized under a given mass constraint, it is not possible to provide a specific upper value of the total mass (with or without the matching cost weighted). Therefore, the commonly used single-objective compliance minimization problem under a mass constraint cannot be used. So, we use the mass minimization problem subject to a constraint on thermal compliance, although the constraint value $\mathcal{C}^*$ of thermal compliance $\mathcal{C}$ remains to be determined:

Formulation 1

$$\underset{\boldsymbol{\rho}}{\text{minimize}} \qquad \mathcal{M}(\boldsymbol{\rho}) \tag{3.7}$$

$$\text{subject to} \qquad \mathcal{C}(\boldsymbol{\rho}) - \mathcal{C}^* \leq 0 \tag{3.8}$$

where $\boldsymbol{\rho} = \{\rho_1, \rho_2, \cdots, \rho_{N_e}\}^T$. Note that the mass must be weighted by matching cost, and can be written in compact form as

$$\mathcal{M}(\boldsymbol{\rho}) = \boldsymbol{\rho}^T \mathbf{W} \tag{3.9}$$

where $\mathbf{W}$ is the vector of the weighting factor, defined as $\mathbf{W} = \{\mathrm{W}_1, \mathrm{W}_2, \cdots, \mathrm{W}_{N_e}\}^T$. To acquire natural-looking seams, thermal compliance

minimization is relaxed to the inequality constraint (3.8). $\mathcal{C}(\boldsymbol{\rho})$ is defined as

$$\mathcal{C}(\boldsymbol{\rho}) = \boldsymbol{\theta}^T \mathbf{K}(\boldsymbol{\rho})\boldsymbol{\theta} \tag{3.10}$$

Although Equation (3.10) represents the stored thermal energy in the thermal system, it corresponds to compliance when the external force $\mathbf{F}$ is constant. Therefore, we use Equation (3.10) to represent thermal compliance. In this equation, the stiffness matrix $\mathbf{K}$ of the system is assembled by using the element-level stiffness matrix $\mathbf{K}_{\mathbf{e}}$, which can be expressed as follows:

$$\begin{aligned} \mathbf{K}_{\mathbf{e}}(\rho_{\mathrm{e}}) &= \rho_{\mathrm{e}}^{p}\mathbf{K}_{\mathbf{e},0} \\ \mathbf{K}_{\mathbf{e},0} &= k_e\mathbf{K}_0 \end{aligned} \tag{3.11}$$

where p is the penalty exponent chosen to ensure convergence to the distinct 0–1 density field as used in the SIMP (solid isotropic material with penalization) approach [1]. Because p should be greater than one, we choose $p = 3$ in this study. While $\mathbf{K}_{\mathbf{e},0}$ is the density-dependent element stiffness matrix, $\mathbf{K}_0$ is the density-independent element stiffness matrix (corresponding to $\rho_e = 1$), which in this case is simply $\begin{bmatrix} 1 & -1 \\ -1 & 1 \end{bmatrix}$. Symbol k stands for thermal conductivity, and we simply assume $k = 1$.

To use the formulation given by Equations (3.7) and (3.8), the upper limit $\mathcal{C}^*$ should be properly chosen, but it is not possible to determine its exact value because the value is problem dependent. Setting the value of $\mathcal{C}^*$ is critical to making the formulation work. We thus propose double-loop topology optimization, in which $\mathcal{C}^*$ is automatically updated during optimization iterations. To update the design variables iteratively by a numerically efficient sensitivity-based optimizer, we need to derive the design sensitivities of the objective and constraint functions. If a sensitivity analysis is carried out with respect to the design variable ρ_e, one can find

$$\frac{\partial \mathcal{M}}{\partial \rho_{\mathrm{e}}} = V_{\mathrm{e}} \tag{3.12}$$

$$\frac{\partial \mathcal{C}}{\partial \rho_{\mathrm{e}}} = -\boldsymbol{\theta}_{\mathbf{e}}^{T} \frac{\partial \mathbf{K}_{\mathbf{e}}}{\partial \rho_{\mathrm{e}}} \boldsymbol{\theta}_{\mathbf{e}} = -p \rho_{\mathrm{e}}^{p\text{-}1} \boldsymbol{\theta}_{\mathbf{e}}^{T} \mathbf{K}_{\mathbf{e},0} \boldsymbol{\theta}_{\mathbf{e}} \tag{3.13}$$

where $\mathbf{T_e}$ is the element temperature vector consisting of node temperatures at both ends of an element.

For conventional topology optimization problems, a reversed form of Formulation 1 which minimize the compliance subject to a limited mass may be used as follows,

Formulation 2

$$\underset{\boldsymbol{\rho}}{\text{minimize}} \qquad \mathcal{C}'(\boldsymbol{\rho}) \tag{3.14}$$

$$\text{subject to} \qquad \mathcal{M}'(\boldsymbol{\rho}) - \mathcal{M}^* \le 0 \tag{3.15}$$

Here the mass term is given by $\mathcal{M}'(\boldsymbol{\rho}) = \boldsymbol{\rho}^T \mathbf{V}$ with the volume vector $\mathbf{V} = \mathbf{1}$ and it is still hard to choose the mass upper bound $\mathcal{M}^*$. The compliance term is rewritten as $C'(\boldsymbol{\rho}) = \boldsymbol{\theta}^T \mathbf{K}'(\boldsymbol{\rho})\boldsymbol{\theta}$ where $\mathbf{K}'$ is the system stiffness matrix for the system. Because, to apply this formulation to our problem, we need to assume the one-dimensional elements with the same length and volume of 1, but with different thermal conductivity k_e according to the matching cost M_e. A penalized form of $k_e = \left(1/M_e\right)^r$ with the exponent $r > 1$ is used to amplify the effect of inverse relation and the penalty exponent $p = 3$ is used. That is, the element-level stiffness matrix $\mathbf{K}_e'$ constituting $\mathbf{K}'$ is obtained in the same way in Equation (8) except $k_e = \left(1/M_e\right)^r$. However, using both of these exponents p and r in calculating $\mathbf{K}'$ causes computational instability in the optimization process. As a result, the convergence of the design variables is impeded or it is easy for the objective function to converge to the local minima.

To avoid these numerical problems, we finally set up our topology optimization problem based on Formulation 1. We use the method of moving asymptotes (MMA) [50] as an optimizer. The algorithm using Equations (3.7) through (3.13) can be summarized in the following pseudocode, which we will call Algorithm 1:

Algorithm 1: Topology optimization to find the outline of the heat path

---

Input: the vector of the weighting factor $\mathbf{W}$, the upper bound of constraint $\mathcal{C}^*$

Output: design variable $\boldsymbol{\rho}$, heat flux $\mathbf{q} = \{q_1, q_2, \cdots, q_{N_e}\}^T$

while criteria for convergence of design variables or objective function are not satisfied **do**

calculate $\boldsymbol{\theta}$ from $\mathbf{K}\boldsymbol{\theta} = \mathbf{F}$

calculate the objective function $\mathcal{M}(\boldsymbol{\rho})$ and the constraint $\mathcal{C}(\boldsymbol{\rho}) - \mathcal{C}^*$

calculate the design sensitivities for $\mathcal{M}(\boldsymbol{\rho})$ and $\mathcal{C}(\boldsymbol{\rho}) - \mathcal{C}^*$

calculate heat flux $\mathbf{q}$

update $\boldsymbol{\rho}$ using design sensitivities by MMA

end while

3.3.2 Strategies for implementation of topology optimization

We present some strategies in addition to the formulation proposed above to implement topology optimization successfully for image stitching. The optimized path should be a single line to stitch two images. Specifying the optimized result is not general in topology optimization, so additional condition is required for convergence to a single line. Even this condition is related to the constraint condition of Formulation 2. Also we propose a two-loop algorithm that performs topology

optimization several times and updates the constraints at each time because the optimized path does not converge well to a single line through one time of optimization in this problem.

Converging of the path to a single line

It is necessary that the optimized heat path is a single line to be a seam for image stitching. The single line means a kind of serial connection in which each node of an element is connected to only one node of the other element. In conventional topology optimization there is a constraint for the resource such as volume or mass, but it is far from a condition for serial connection.

As shown in Figure 3.8, both a single line and multipath of the same length can be candidates for the optimal path if image stitching is not considered. The goal of topology optimization is to derive the solution that has the minimum value of the objective function subject to the constraints regardless of whether serial or parallel connections. However, in present research, the constraint that the heat path should be connected in series is additionally required for image stitching. This has not been generally addressed in the topology optimization design so far and difficult to be expressed in the constraint condition. There are some studies that have attempted to control the formation of a solution in the existing topology optimization studies, for example, a research to derive specific configuration such as a thin line has been carried out. However, most of the researches are about filters applied in the

continuum model and there is nothing about controlling the configuration of the solution in the ground structure model. We approach this in a way other than filter by using an inherent condition in the constraint.

Let's take the concept of thermal resistance and consider the equivalent thermal circuit of a thermal conduction system as shown in Figure 3.9. The left is the circuit connected only in series and the right side is the circuit connected only in parallel. Thermal resistance R is a property that means the degree of resistance to heat flow expressed as

$$R = L / kA \tag{3.16}$$

where A and L are the area of the cross section and the length of the heat conductive element, respectively. Because we assumed that all elements are one dimensional and have same length, we only consider the inverse relation between the thermal resistance and the conductivity. As we aim to obtain a serially connected heat path, we first examine the difference in total thermal resistance R, equivalent thermal conductivity k_{eq}, and thermal compliance $\mathcal{C}$ of the thermal circuit between the serial and the parallel thermal circuit consisting of n elements as summarized in Table 3.2.

For the analysis, we assume that the heat flux q_{eq} from a heat source to a heat sink in the two cases is the same and the number N_q of heat conduction elements forming the heat paths is also identical for the two thermal circuits. Note that the thermal compliance expressed as Equation (3.10) can be simply expressed as $\mathcal{C} = q_{eq}^2 / k_{eq}$ if the equivalent thermal conductivity k_{eq} for any path is known. Because $k_{eq,series} = k / N_q$ for the serial connection and $k_{eq,parallel} = N_q k$ for the parallel connection, the corresponding compliances are $\mathcal{C}_{series} = N_q q_{eq}^2 / k$ and $\mathcal{C}_{parallel} = q_{eq}^2 / N_q k$, respectively. Thus, the following relation always holds for $N_q > 1$.

$$\mathcal{C}_{series} > \mathcal{C}_{parallel} \tag{3.17}$$

This is means that the compliance for parallel or partially parallel connections is always less than for a fully serial connection. Therefore, the compliance of the heat system should become large to obtain a single line.

Setting the upper bound of the constraint condition

In Section 3.3.1, we mentioned difficulties in setting the upper bound of the constraint condition of both Formulation 1 and 2. For example, using Formulation 2 in general aims to find the best configuration of the material under limited mass

which is represented by the constraint condition, and SIMP is an essential part to implement the topology optimization method. However, if the amount of resource is not given, we are not able to use the conventional formulations base on SIMP that has been studied so far. The problem of difficulty in setting the available mass also can be found in several topology optimization research, such as researches on the synthesis of linkage mechanism [4] or the metamaterial design [8]. Especially, in optimization study on finding heat paths for the robot path planning [15], they adopted a strategy that reduces the upper bound in a mass constraint for each iteration. However, this method did not work well for our problem. We eventually adopted Formulation 1 where minimizing the mass and the thermal compliance are used as the objective function and the constraint condition, respectively, for the reasons discussed in Section 3.3.1. There is a tradeoff relation between the mass and compliance. In the mass minimization setup here, that is, mass minimization without any constraint on compliance should result in an increase in compliance value. Therefore, the compliance for the serial connection $\mathcal{C}_{series}$ which is the maximum value for the connected paths with the same length should be the upper limit $\mathcal{C}^*$ of the compliance constraint. When the thermal conductivity k of all elements are 1 and the heat flux q_{eq} of the total system is 1 the upper bound $\mathcal{C}^*$ can be rewritten as

$$\mathcal{C}^* = N_q \tag{3.18}$$

where N_q is the number of elements composing the serially connected path. Equation (3.18) is the compliance upper bound as well as an implicit condition that induces a series connection by itself.

Nevertheless, it is still difficult to know the exact number of elements of the single path to be formed. This can be approximated as the number of elements along which the value of the element's heat flux is greater than a threshold value $q_{threshold}$; the heat conduction elements along the optimized heat path should have meaningful amounts of heat flux. We use $q_{threshold} = 0.01$. To calculate heat flux q_e in each element, we use

$$q_e = \rho_e^3 \Delta T_e \tag{3.19}$$

where ΔT_e is the temperature difference between nodes forming the *e*th element. At the beginning of topology optimization, we start with the same value of ρ_e. Therefore, we cannot use the threshold value. In this case, we set N_q equal to the total number of elements that contribute to forming a monotonically increasing zigzag line from the top-left corner node to the bottom-right corner. This amounts to the sum of the width and height of the design domain (in case of the example shown in Figure 3.8, the initial value of N_q is 6.)

Double-loop algorithm

Even though using Formulation 1 with Equation (3.18) for the constraint, a single line for image stitching is not always guaranteed through the only one time of topology optimization. In order to compensate this point, we propose an algorithm which is divided into double loops: the first is an inner loop which is topology optimization to find the outline of the heat path (Algorithm 1) and the second is an outer loop which repeats optimization process to improve the convergence of the heat path (Algorithm 2). At the start of each optimization process, the upper bound of the compliance $\mathcal{C}^*$ and the vector of the weighting factor $\mathbf{W}$ of the objective function should be updated. The initial value of N_q is assumed a sum of vertical and horizontal lengths of the design domain and after that, is obtained newly by counting the number of elements having valid heat flux values among the total elements at the previous process. In addition, the vector of the weighting factor $\mathbf{W}$ in the objective function is penalized by heat flux. These two key parameters are updated as follows

$$\mathcal{C}^{*\,(J)} = N_q^{\,(J-1)} \tag{3.20}$$

$$W_e^{\,(J)} = W_e^{\,(J-1)} / q_e^{\,(J-1)} \tag{3.21}$$

where symbol J in Equations (3.20) and (3.21) denotes the index representing the number of iterations in Algorithm 2. The role of Equation (3.21) is to penalize weight

W_e by using the heat flux flowing in the *e*th element. With this scheme, weight W_e in elements with small heat flux flows becomes larger and is thus avoided in subsequent iterations. This technique is also effective to push the heat path to form a single-line path because the weights increasingly contrast. Through the iterative optimization process, the elements having a valid heat flux among all the elements are filtered step by step. Our double-loop algorithm is finally terminated when certain criteria are satisfied within a maximum number of outer iterations. Stitching using the proposed topology optimization method is mainly performed on two patches, and can be repeated if image synthesis involves several patches. Algorithm 2 can be summarized in the following pseudocode and the flowchart of Figure 3.10.

Algorithm 2: Double-loop algorithm for converging to a single line

---

$W_e^{(0)} = (M_e)^2$, $q_e^{(0)} = 1$

$N_q^{(0)} \leftarrow$ sum of the width and the height of the design domain

for $J = 1 : J_{\max}$ **do**

  $W_e^{(J)} \leftarrow W_e^{(J-1)} / q_e^{(J-1)}$

  $C^{*(J)} \leftarrow N_q^{(J-1)}$

  Run Algorithm 1 for stage J

  $\mathbf{q}^{(J)} \leftarrow$ Algorithm 1($\mathbf{W}^{(J)}$, $C^{*(J)}$)

  $N_q^{(J)}$: The number of $q_e^{(J)}$ satisfying $q_e^{(J)} > q_{threshold}$

  if the optimal path converges to a single line **then**

    break

  end if

end for

3.4 Stitching for two patches

3.4.1 Validation Examples for simple two patches

As the first validation example, we consider stitching two patches consisting of monotonic 80×80 pixels with a rectangular overlap area of 20×80 pixels, as shown in Figure 3.11. Patches A and B have the same color but Patch A has a partially shaded zigzag region in the overlap region. The overlap region is the design domain for the topology optimization of the heat transfer system, and a heat source and a sink are located above and below the design domain. In calculating the matching cost, Equation (2.4) mentioned in Chapter 2 was used, which takes into account the gradient information of the image. With considering the gradient of the image, the optimal path coincides the zigzag area of Patch A, while without considering that one, the optimal path is a straight line, a trivial solution. By considering the gradient information of the image, the contents of images can be preserved in the process of stitching patches. The optimization history is shown in Figure 3.12. The results show that convergence was reached after 40 iterations, in which three outer loops were run through three stages: Stage 1 with an upper bound of $\mathcal{C}^* = \mathcal{C}^{*(1)}$, Stage 2 with $\mathcal{C}^* = \mathcal{C}^{*(2)}$, and Stage 3 with $\mathcal{C}^* = \mathcal{C}^{*(3)}$. Although the initial value of $\mathcal{C}^*$ is arbitrarily assumed as the sum of the width and height of the design domain, it is slightly different from the final value of that. In addition, through proper updating scheme of $\mathcal{C}^*$, the optimization is successfully performed. Due to the characteristics of the MMA, the sensitivity-based optimizer, compliance as a constraint equation

reaches its upper limit $\mathcal{C}^*$ before the matching cost-weighted mass (objective function) is primarily minimized. In the plot showing the evolution of the heat path, all finite conducting elements with $\rho_e \geq 0.1$ are plotted. The first process takes the greatest proportion of the entire optimization process. In this process, a rough outline of the optimal path is obtained, but this path is a multiple path which has several sub-paths because they cannot converge to a single line yet. In the second process, the optimization is repeated with updating the upper bound of the mass and the constraint of the objective function. As a result, unnecessary paths disappear and converge to a single line. In the third process, the path does not change, but the design variables converge to 0 or 1 completely.

The shape of the optimal path on the left is same as the boundary line of the shaded region of patch A. We can find that the optimal path is formed along the line with large differences of the pixels (the shaded region). If the matching cost was defined differently as, instead of Equation (2.4),

$$M(s,t,\mathbf{A},\mathbf{B}) = \left\|\mathbf{A}(s)-\mathbf{B}(s)\right\| + \left\|\mathbf{A}(t)-\mathbf{B}(t)\right\| \tag{3.22}$$

then the optimal path would be a straight vertical line where the path is the shortest because gradient information ($\left\|G_{\mathbf{A}}^{d}\right\|$ and $\left\|G_{\mathbf{B}}^{d}\right\|$) is not used. In both cases, patches are stitched well in the result image. However, in general images, not monotonous

like this example, image stitching can be performed better while preserving the contents of images when considering the gradient of the image. For all of the examples in this section, the gradient information has been taken into account.

In order to stitch various patches for texture synthesis, it is necessary to consider the overlap region of irregular shapes as well as regular shapes. In case for patches of different sizes as shown in Figure 3.13, the overlap region could be L-shaped. Even in this case, this area is a design domain for optimization, and the source and sink are located at both ends of the design domain. Patch A is 140×140 pixels, patch B is 80×80 pixels, and the width of the overlap region is 20 pixels. The optimized path is shown at the bottom left of Figure 3.13. This path is also identical to the boundary line of the shaded area in patch A. We can find that the proposed algorithm finds the path that minimizes the matching cost while preserving the image contents even when the shape of design domain is not regular.

The following example is for two patches with random colors within a specific range. In Figure 3.14, both of two patches have a shaded area in the overlap regions. The optimized path is also identical with the boundary line of the shaded area of the patches and the two patches are smoothly stitched like as in the resulting image. We can find that the proposed algorithm work well for images with random pixels. In addition, our algorithm does not restrict the directionality of paths. In the optimized path of Figure 3.14, the shape of the path is formed by changing the direction up and

down not in one direction. This clearly shows that our algorithm works for a path with a reversed path segment along it, suggesting its versatility.

3.4.2 Stitching results for two patches of general images

We applied the proposed method to stitch more general images shown in Column A in Figure 3.15. The optimized seams for the stitched images are presented in Column B of Figure 3.15 as white lines while the synthesized images without illustration of the seams are shown in Column C. Images of different types and sizes (stated in the caption of Figure 3.15) were considered to demonstrate the versatility of the proposed algorithm, and it successfully yielded single-line seams with natural appearance for all problems considered.

Of the three cases considered in Figure 3.15, the patch stitching high-resolution image in the first row is examined in detail. Figures 3.15–3.17 are the results of this case. From Figure 3.16, we find that the objective function (matching cost-weighted mass) decreases gradually with each stage J as topology optimization proceeds. The weight vector $\mathbf{W}$ and upper bound of compliance C^* were updated for each stage J following the rules given by Equations (3.20) and (3.21). As a result of updating, some jumps occur in the objective function when the outer loop stage changes. In Stage 1, the heat path was complex with multiple, multiply connected line segments, but the outline of the optimal path appeared to have been formed. The single-line

path started to appear in Stage 3 but the design variables were pushed toward the converging states of zero and one. See the distributions of the design variables at iterations in Figure 3.17. This means that later stages mainly served for the convergence of the design variables without affecting the optimized heat path. Figure 3.18 shows the detailed evolution history of the seam during topology optimization process.

Figures 3.19, 3.20, and 3.21 show the results for the three other cases in Figure 3.15. The rate of convergence varied from one case to another, but the overall behavior of the optimization process was the same. This implies that the proposed method performed equally for different kinds of images. Finally, we considered stitching two patches of different shapes shown on the left side of Figure 3.22. The synthesized result is shown on the right side while the convergence history is given in Figure 3.23.

3.5 Texture Synthesis for general images

We applied the proposed algorithm to form large images from small source images. In doing so, patches with the least difference in the overlap region were chosen sequentially from the source image once the first patch had been randomly picked, as in Efros and Freeman [24]. They are shown in Figures 3.24, 3.25, and 3.26. For all cases considered here, all patches were square and the width of the overlap region was equal to a quarter of the width of the patches to be stitched. Depending on the images, the sizes and the number of patches that formed the synthesized images were not the same. When patches were stitched along a seam, a smoothing filter was used to compensate for some artifacts that might have occurred, even though the optimal seam was obtained through the optimization process. For Figure 3.24, the patch size varied from 40×40 to 80×80 pixels while the number of patches composing the final image varied from 5×5 to 10×10. For all cases considered in Figure 3.25, the patch size and number of patches were 40×40 pixels and 10×10, respectively. For all cases in Figure 3.26, the patch size and the number of patches were 40×40 pixels and 14×14, respectively. The source images in Figure 3.26 were taken from images created by the variational art algorithm [16] (these images were generated to form a regular pattern when they were connected). The cases considered in Figures 3.23 to 3.25 clearly demonstrate the versatility and effectiveness of the proposed image stitching algorithm.

3.6 Time complexity

The proposed algorithm is based on topology optimization, and is divided into matrix assembly for system analysis, solving the matrix equation, objective function, sensitivity analysis and filtering. The process of solving determinants in the computational complexity of topology optimization is the dominant part. The mathematical complexity of LU decomposition for solving this linear system is $O(\mathrm{n}^2)$, which is known to be reduced to $O(\mathrm{n})$ level through parallel computing. On the other hand, graph-cut, which is widely used in the field of computer vision including texture synthesis, is based on the min-cut / max-flow algorithm. The max-flow algorithm is theoretically known to have the worst-case time complexity of $O(\mathrm{n}^3)$ and is somewhat unsuitable for parallel computing [51]. We compared the execution time of the image stitching problem by referring to the overall characteristics of the two algorithms. However, since the types of coding languages available at present and the degree of optimization of codes are very different, only the tendency to increase in time due to an increase in degrees of freedom is examined. Figure 3.27 shows that the code topology optimization algorithm tends to increase linearly with increasing degrees of freedom. In addition, the amount of increase is slightly reduced in the section where the degree of freedom is relatively large. On the other hand, as the degree of freedom increases, max-flow increases gradually. This means that as the degree of freedom increases, the efficiency of the max-flow algorithm decreases. It also means that the topology optimization algorithm is

efficient for high computational complexity and high degrees of freedom. Therefore, the proposed texture synthesis algorithm is more meaningful when dealing with high-resolution images, and can be an effective alternative in complex computer vision problems than texture synthesis. However, the process of reducing absolute execution time through code optimization is essential.

Table 3.1 Analogy between the path finding in the heat transfer grid structure by topology optimization and the seam finding in graph model by graph-cut algorithm for image stitching.

The proposed method	Graph cut for image stitching
Grid structure model	Graph model
Heat sink	Finish point for cut
Heat source	Start point for cut
Heat-conductive grid elements	Edges of graph model
Weighted mass	Matching cost between pixels
Optimal heat path	Seam for image stitching

Table 3.2 Total thermal resistance R, equivalent thermal conductivity k_{eq}, thermal compliance $\mathcal{C}$ of equivalent thermal circuits with serial and parallel connections. n is the number of elements composing the heat path.

	Thermal circuit in series	Thermal circuit in parallel
R	$R_{total} = R_1 + R_2 + \cdots + R_n$	$\frac{1}{R_{total}} = \frac{1}{R_1} + \frac{1}{R_2} + \cdots + \frac{1}{R_n}$
k_{eq}	$\frac{L}{A} \cdot \frac{1}{k_{eq,series}} = \frac{L}{A}\left(\frac{1}{k_1} + \frac{1}{k_2} + \cdots + \frac{1}{k_n}\right)$ $= \frac{L}{A} \cdot \frac{n}{k}$ $k_{eq,series} = \frac{k}{n}$	$k_{eq} = k_1 + k_2 + \cdots + k_n$ $= n \cdot k$
$\mathcal{C}$	$\mathcal{C}_{series} = k_{eq,series}(\Delta T_{eq})^2$ $= k_{eq,series}(\frac{q_{eq}}{k_{eq,series}})^2 = \frac{q_{eq}^2}{k_{eq,series}}$ $\mathcal{C}_{series} = \frac{q_{eq}}{k_{eq,series}} = \frac{nq_{eq}^2}{k}$	$\mathcal{C}_{parallel} = \frac{q_{eq}^2}{k_{k_{eq,parallel}}}$ $\mathcal{C}_{parallel} = \frac{q_{eq}^2}{k_{eq,parallel}} = \frac{q_{eq}^2}{nk}$

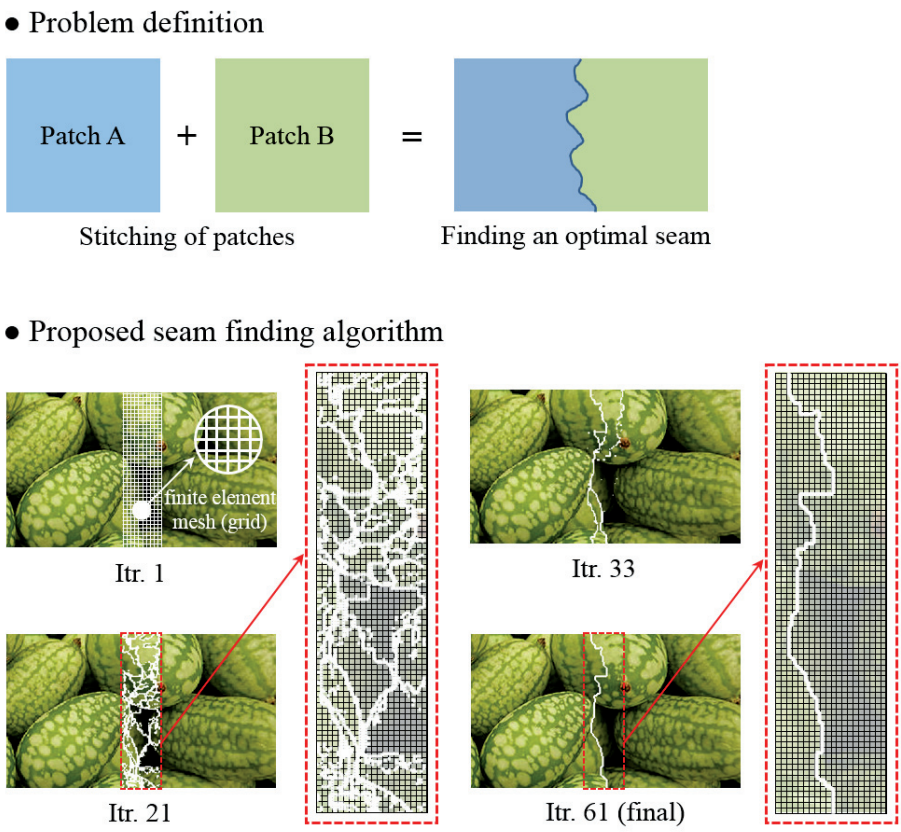

Figure 3.1 The problem definition and an overview of the proposed topology optimization-based algorithm to find an optimal seam for image stitching.

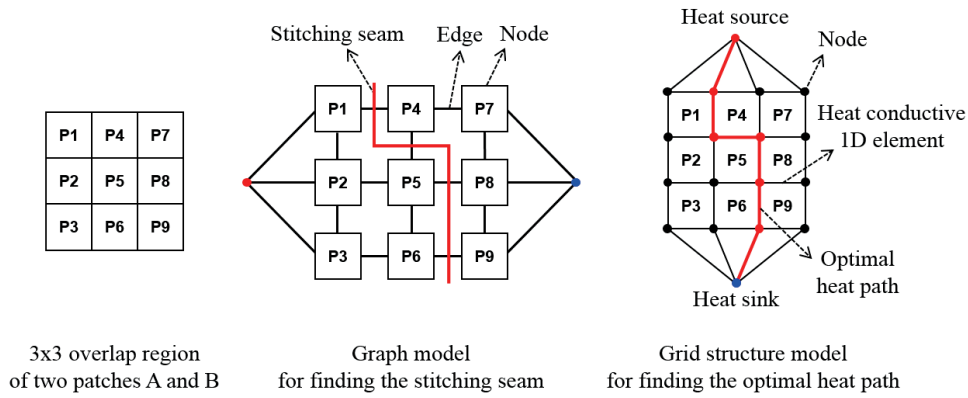

Figure 3.2 The overlap region of 3×3 pixels (left), the graph model of the overlap region consisting of nodes and edges for finding the stitching seam (middle), and the grid structure model of the heat transfer system consisting of 1D heat-conductive elements for finding the optimal heat path (right).

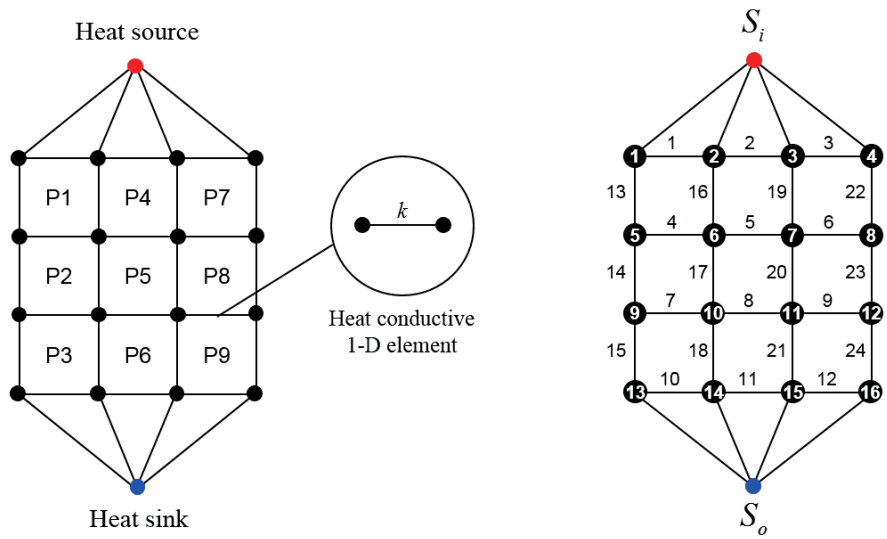

Figure 3.3 The grid structure model for the simulated physical space of heat transfer (left) and the corresponding finite element model (right). They all represent the discretized overall region of the two patches. The numbers inside the black circles denote the node numbers while those next to the lines connecting the node, the element numbers.

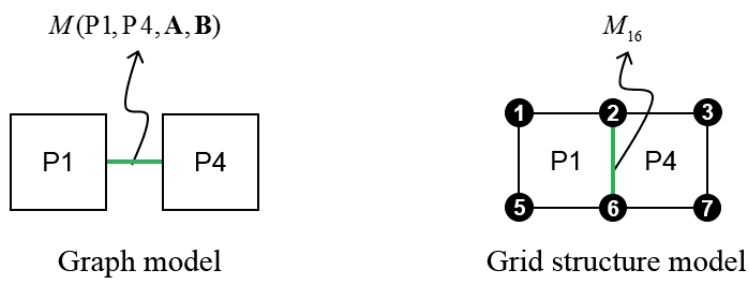

Figure 3.4 Schematic definition of some quantities in the graph model and the grid structure model. The value of the edge conceptually connecting pixels P1 and P4 corresponds to the physical quantity of the element located on the interface between pixels P1 and P4 (green lines). Symbols $\mathbf{A}$ and $\mathbf{B}$ for patches to be stitched are omitted from the notation of the matching cost in the graph model.

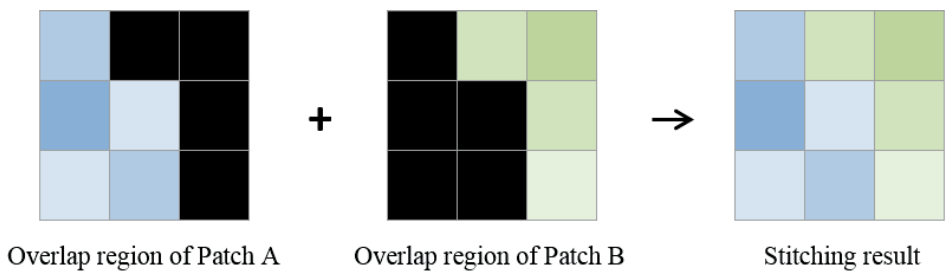

Figure 3.5 Image stitching for an overlap region of 3×3 pixels.

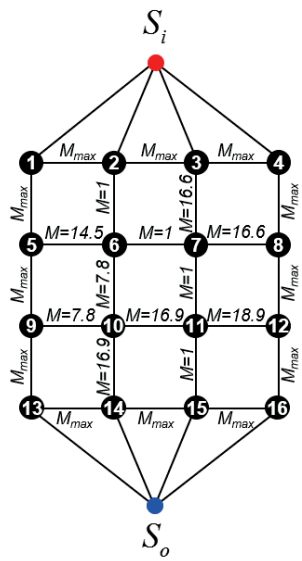

Figure 3.6 The grid structure finite element model for a toy problem, where the grids discretize the overlap region of two 3×3 patches. The outermost elements are assigned a relatively large value of $M_{\max}=10^6$.

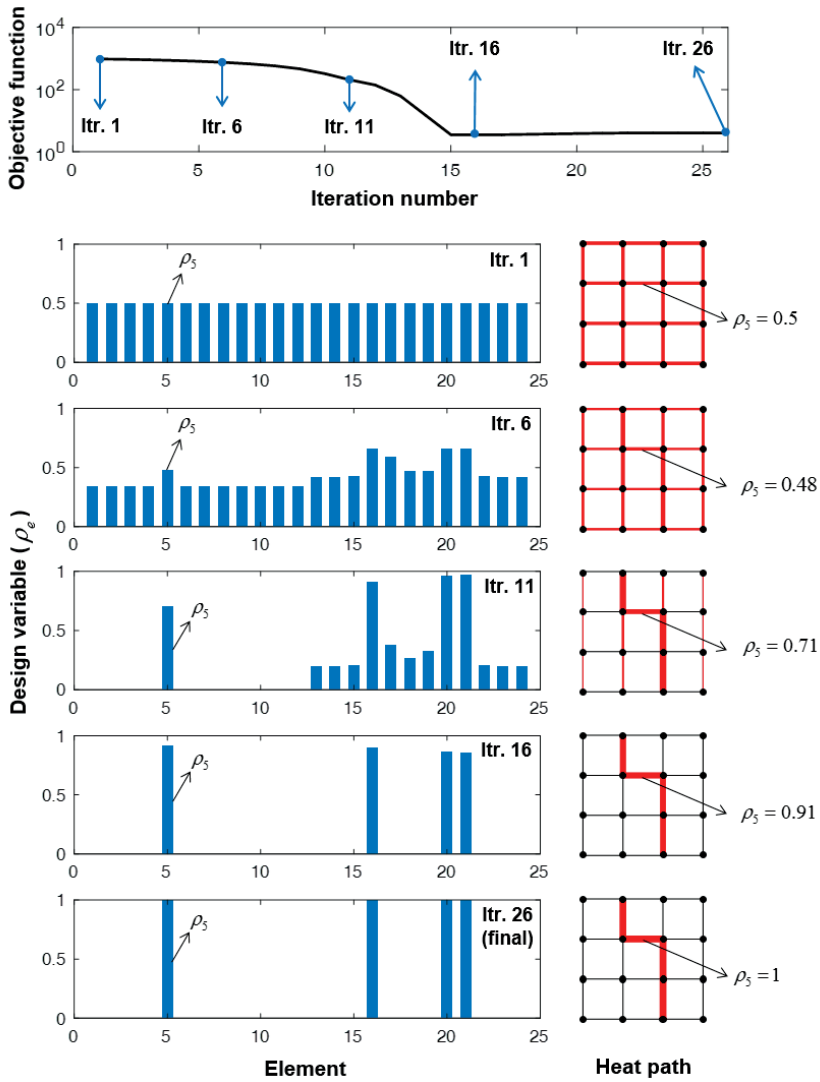

Figure 3.7 An overview of the process of the proposed topology optimization for optimal patch stitching using the toy problem in Figure 3.5. The evolutionary histories of the objective function (top), and design variables and the heat path equivalent to the seam (bottom). The thick red line on the right bottom plot denotes the optimal seam found by the proposed algorithm.

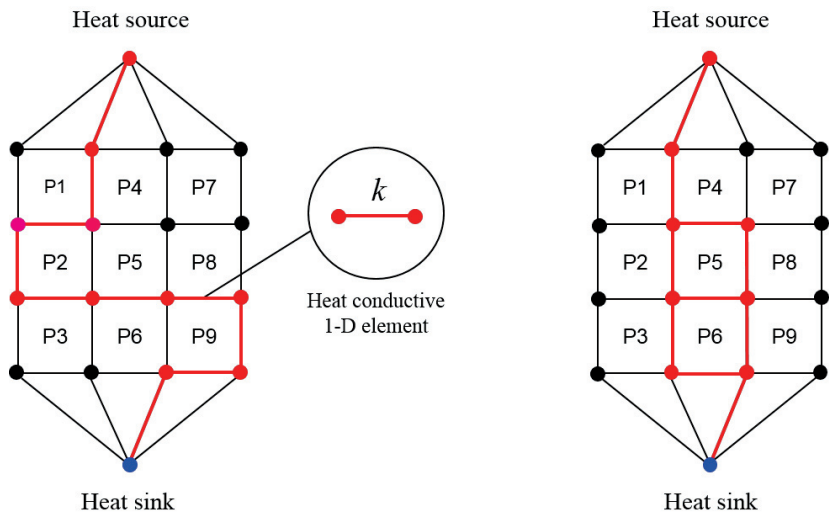

Figure 3.8 A single line (left) and multiple path (right) in a heat transfer system with the same mass. A single line and a multiple path mean a serial connection and a mixture of serial and parallel connections respectively.

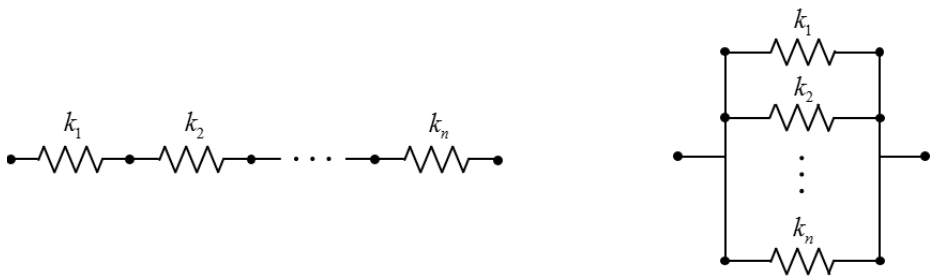

Figure 3.9 Equivalent thermal circuits for heat transfer systems with serial (left) and parallel (right) connections.

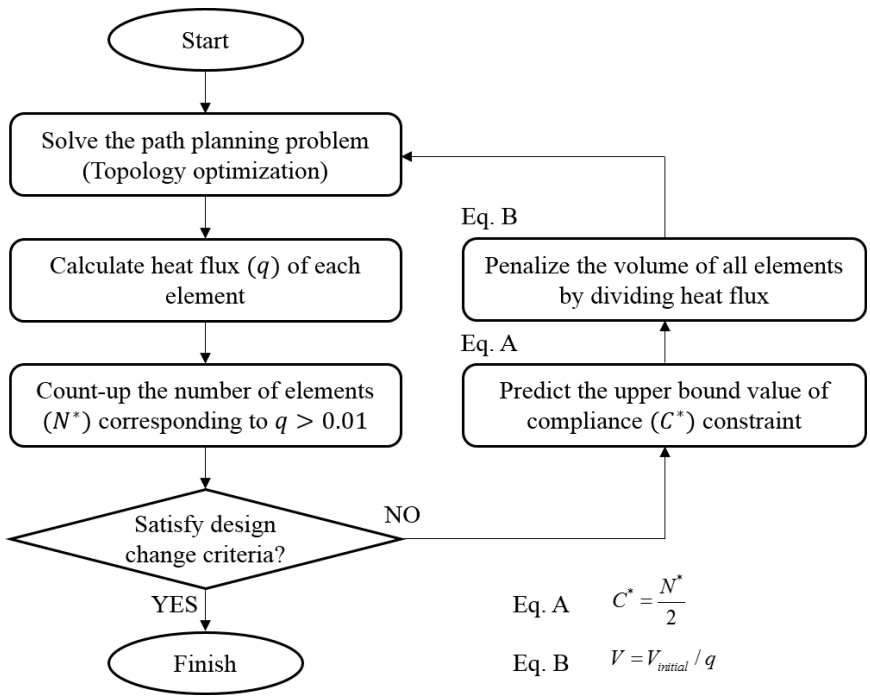

Figure 3.10 Flowchart of the proposed double-loop algorithm.

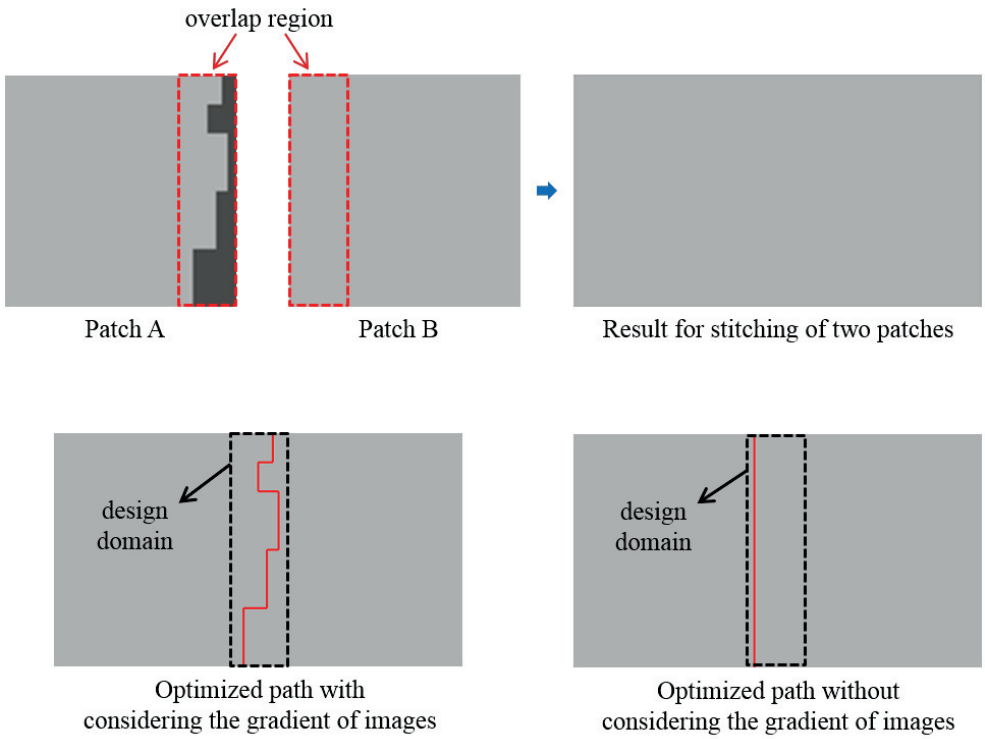

Figure 3.11 Stitching of two simple patches for the cases with (the left of second row) and without (the left of second row) considering the gradient of images. For two cases, stitching results are same but the optimal paths are quite different. Patch A: 80×80. Patch B: 80×80. Overlap width: 20 pixels.

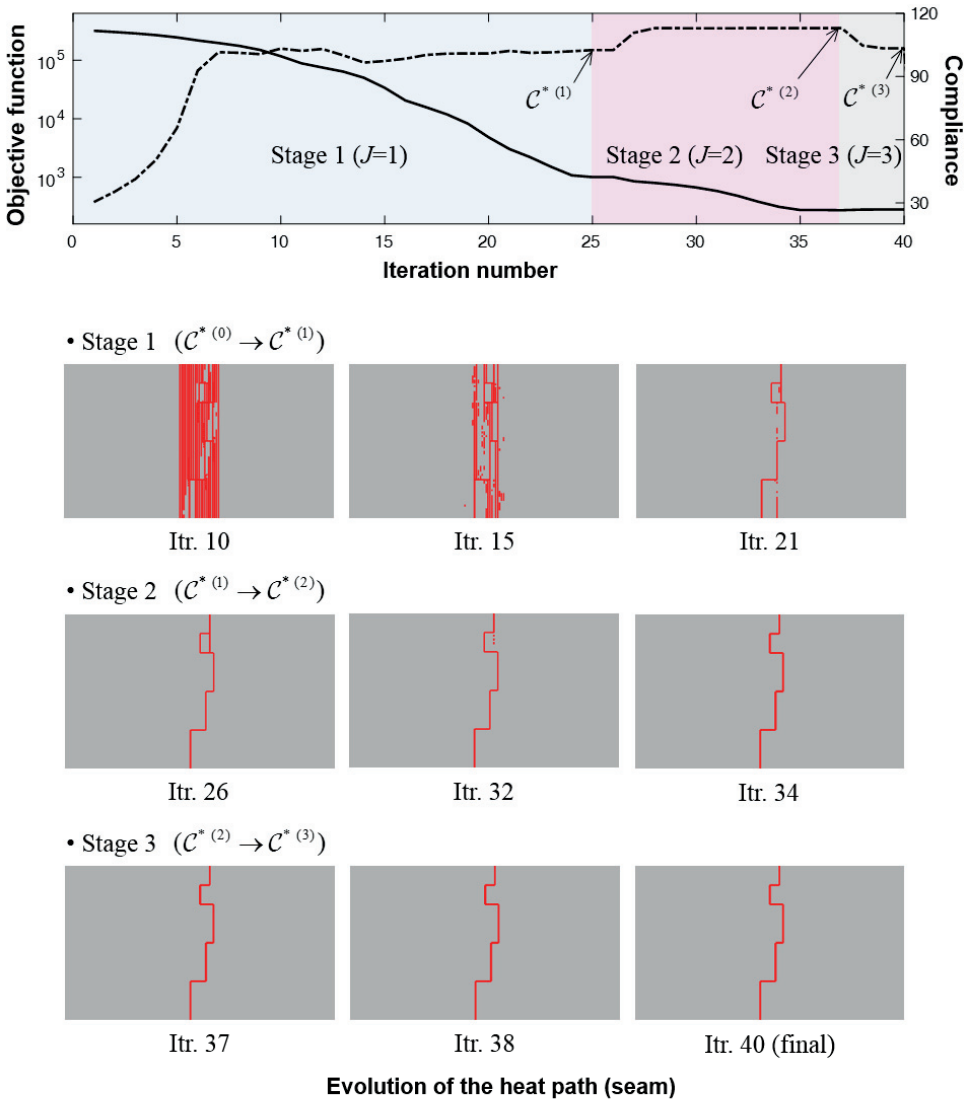

Figure 3.12 The iteration histories of the objective function, which is the matching cost-weighted mass represented by the solid line and compliance represented by the dotted line (top). The evolution of the optimal heat path (i.e., seam) is marked in red. The symbol J represents the outer loop stage index as explained in the pseudo-algorithm.

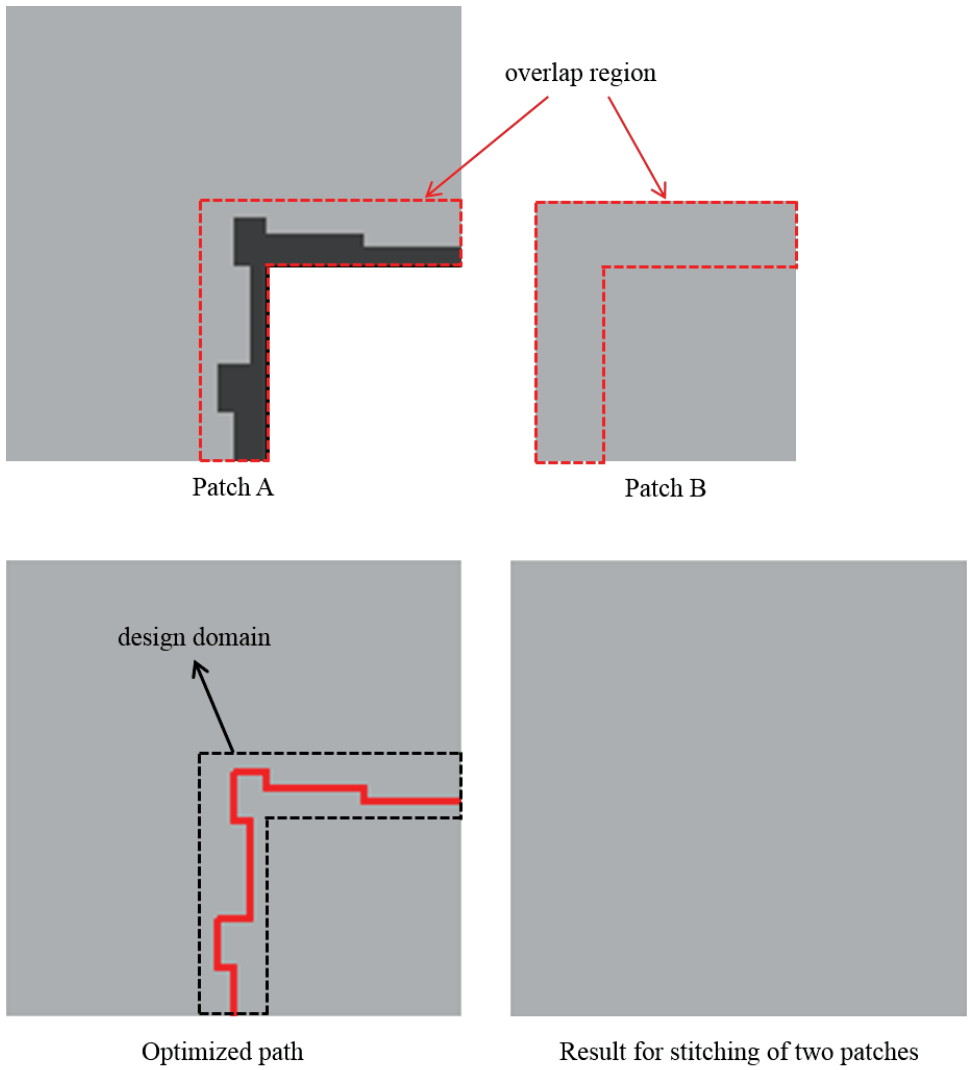

Figure 3.13 Patch stitching with an irregular overlapping region (top). The proposed algorithm correctly yields the optimal path (bottom). Patch A: 140×140. Patch B: 80×80. Overlap width: 20 pixels.

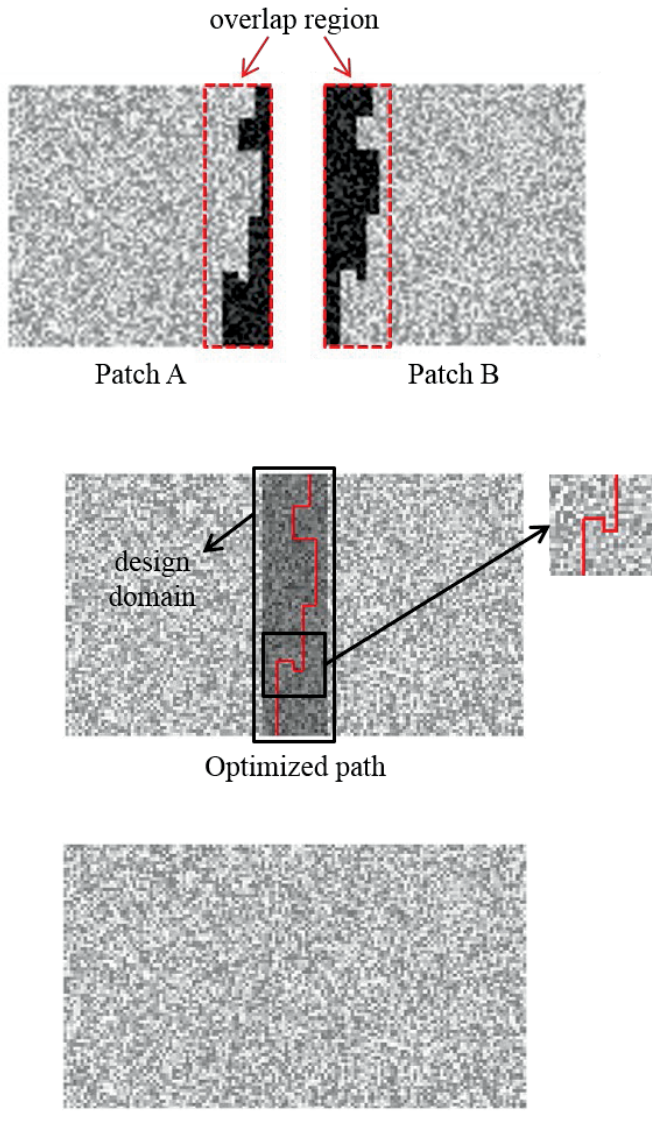

Figure 3.14 The case for the patches with random pixels within a specific range. Patches A and B having a shaded area in the overlap regions, the optimized path and the stitched result are shown in order from the top. Patch A: 80×80. Patch B: 80×80. Overlap width: 20 pixels.

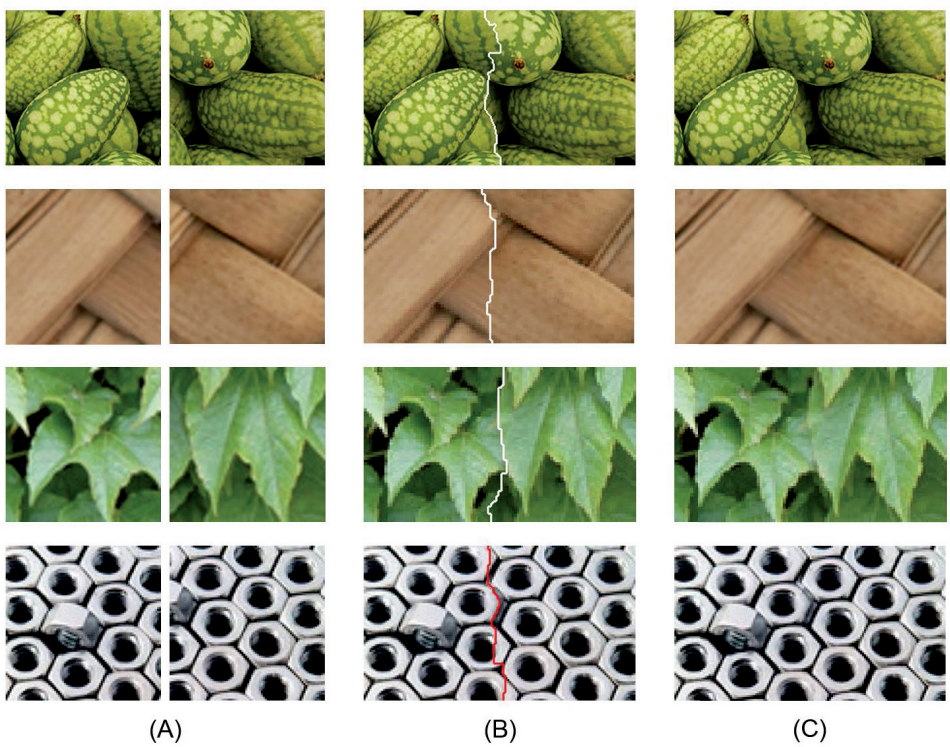

Figure 3.15 Stitching of a pair of general patches. Column A: two patches to be stitched. Column B: stitched images with the optimal paths in the overlap region. Column C: the stitched images without the optimal paths illustrated. Patch pixel sizes from the first row to the last are 160×160, 60×60, 60×60, and 80×80, respectively.

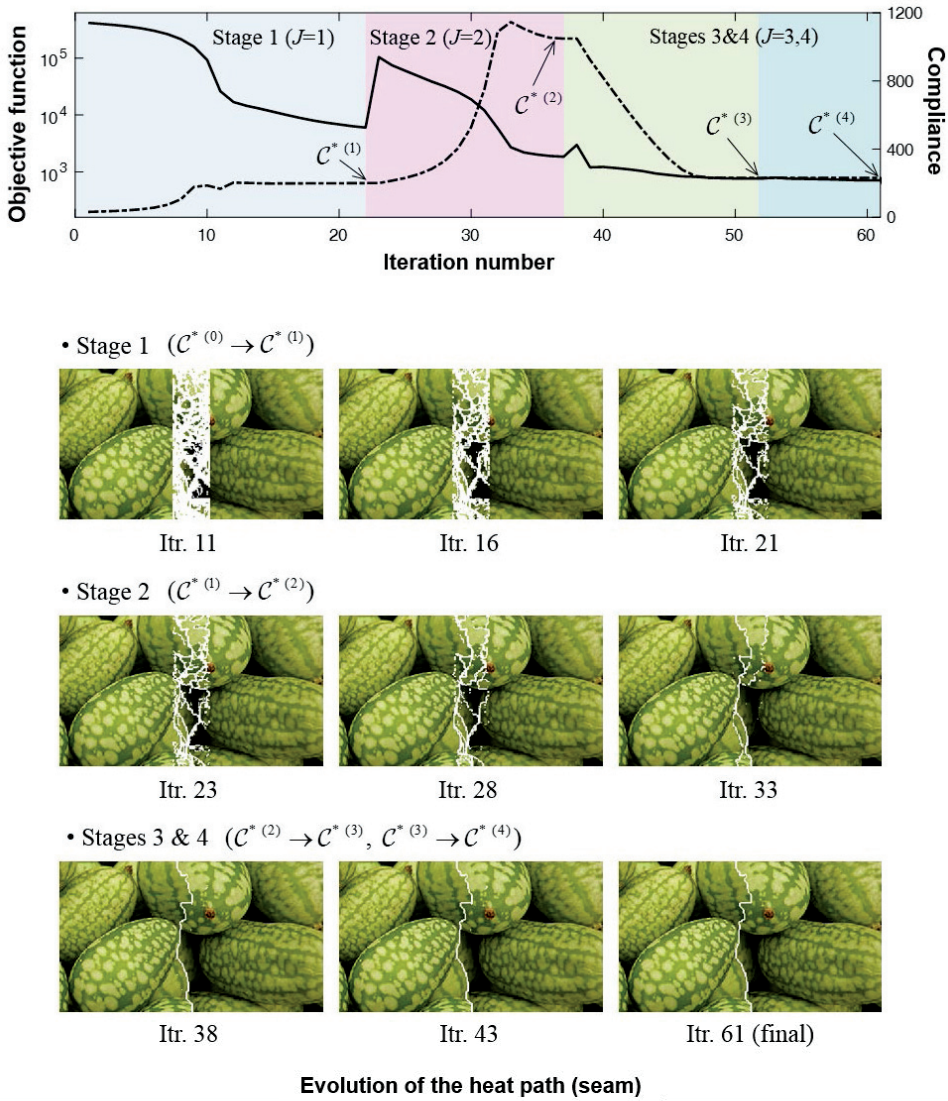

Figure 3.16 Iteration histories of the objective function, which is the matching cost-weighted mass represented by the solid line and compliance represented by the dotted line (top), and the evolution of the optimal heat path (i.e., seam), marked in white for images considered in the first row of Figure 3.15. Symbol *J* represents the outer loop stage index as explained in the pseudo-algorithm.

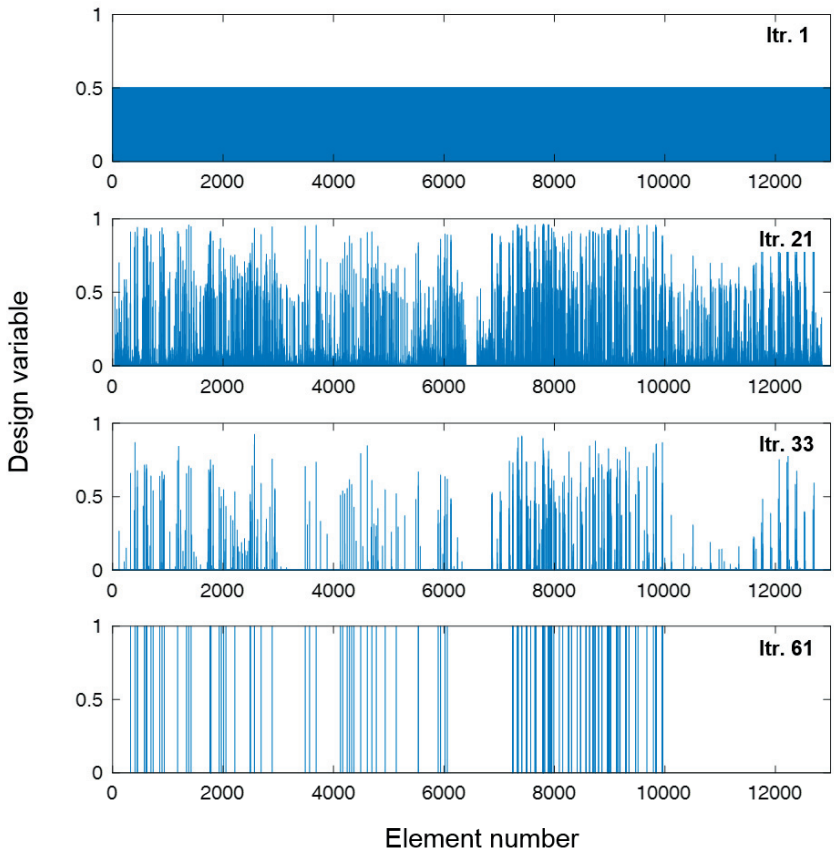

Figure 3.17 Distribution of design variables at iterations 21 (the last iteration of Stage 1), 33 (the last iteration of Stage 2), and 61 (the last iteration of Stage 4) for the image shown in the first row of Figure 3.15. Of 13,000 design variables (elements), 228 having an upper value of 1 participated in the formation of the optimized seam.

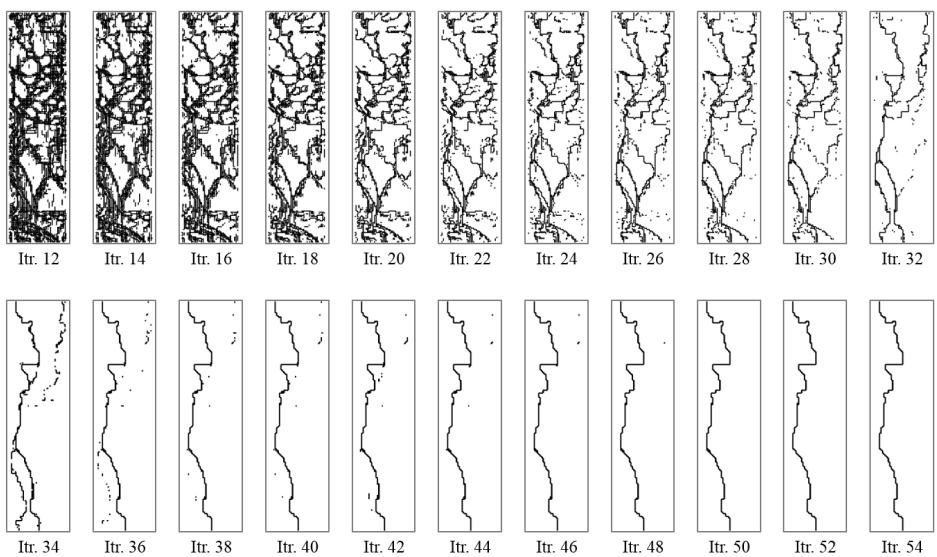

Figure 3.18 More details of the evolution history of the optimized path for stitching images shown in the first row of Figure 3.15 (results before the 12th iteration are not shown here because they were hardly recognized).

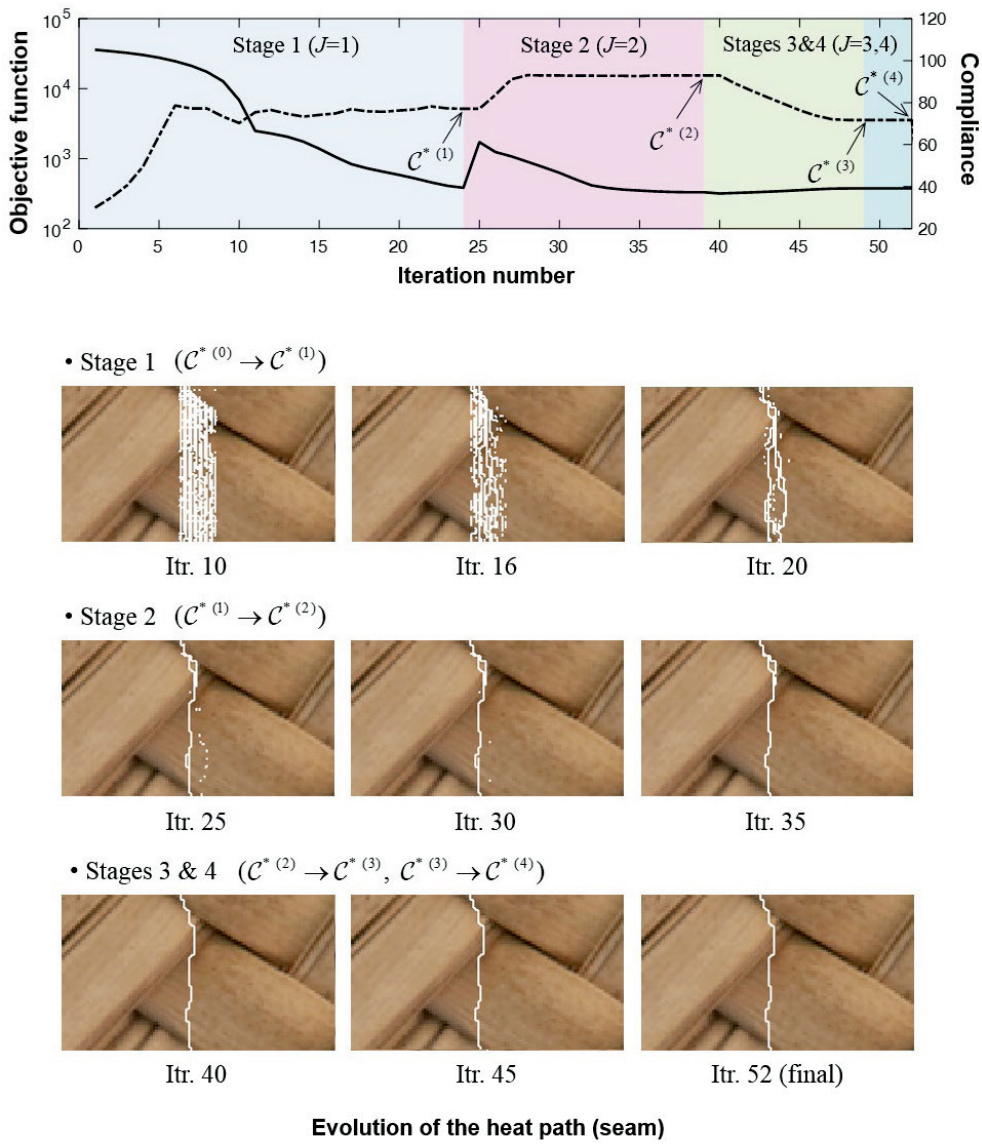

Figure 3.19 Iteration histories of the objective function (solid line) and compliance (dotted line) represented (top), and the evolution of the optimal heat path (i.e., seam), marked in white for images considered in the 2nd row of Figure 3.15 (bottom).

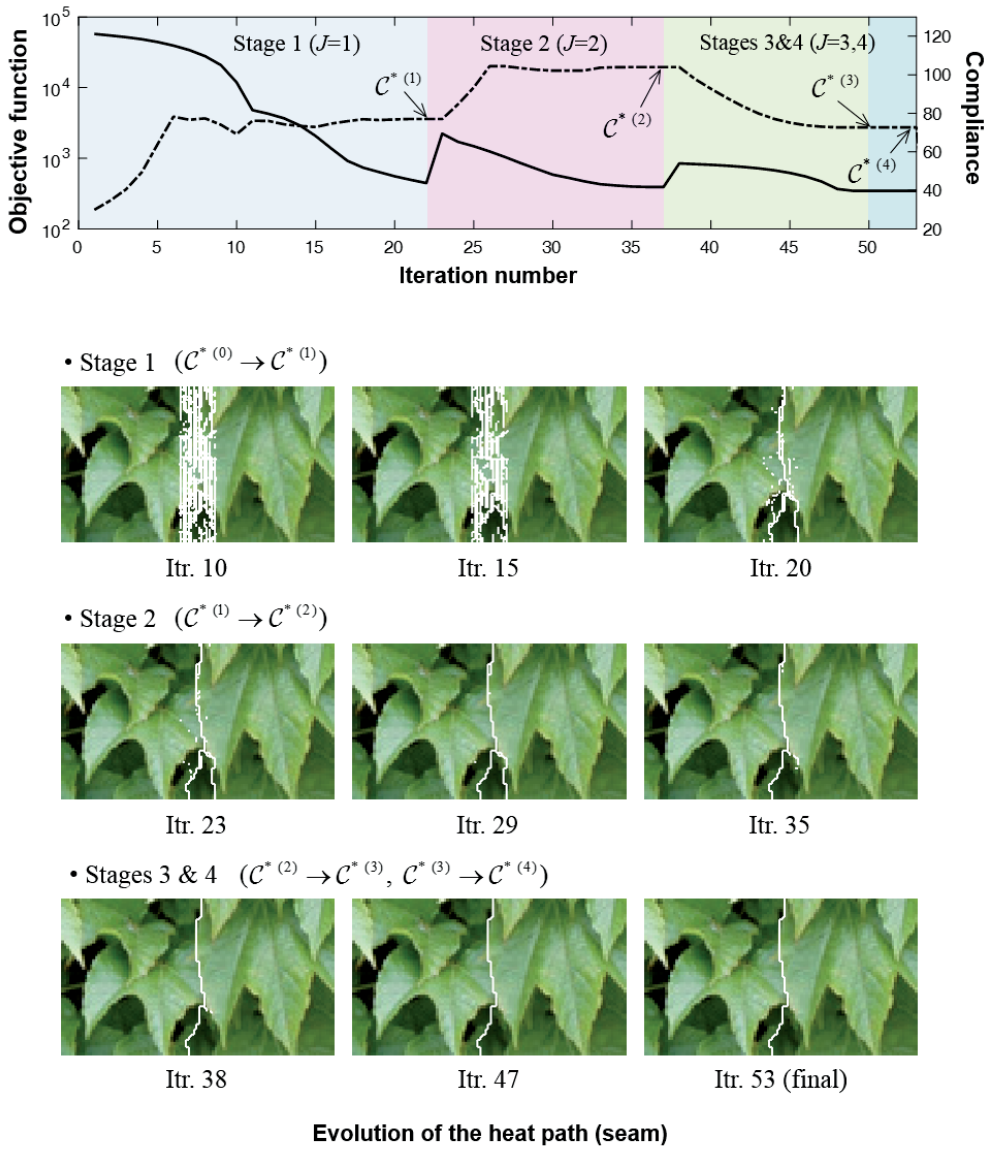

Figure 3.20 Iteration histories of the objective function (solid line) with compliance (dotted line) represented (top), and the evolution of the optimal heat path (i.e., seam) marked in white for images considered in the 3rd row of Figure 3.15 (bottom).

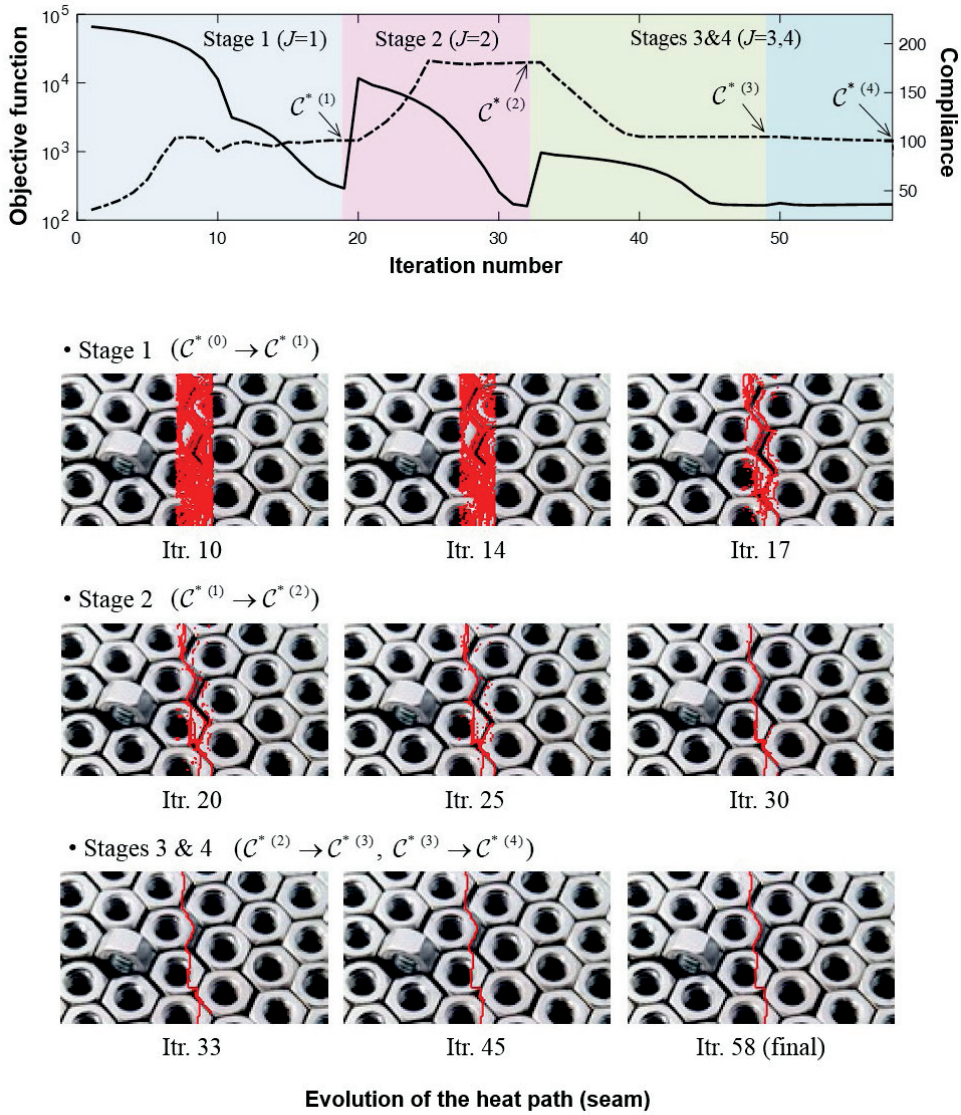

Figure 3.21 Iteration histories of the objective function (solid line) and compliance (dotted line) represented (top), and the evolution of the optimal heat path (i.e., seam) marked in red for images considered in the 4th row of Figure 3.15 (bottom).

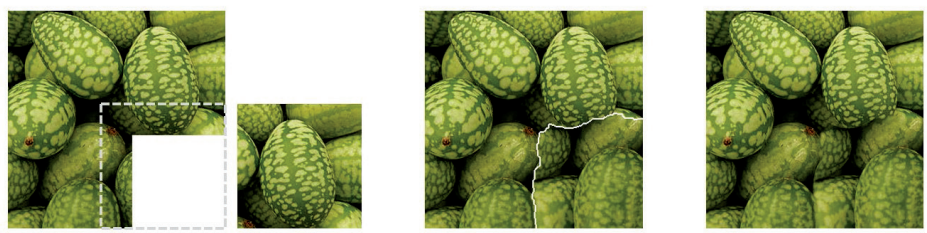

Figure 3.22 Patches with different shapes and sizes (left), and stitched patches with (center) and without (right) the seam illustrated in white. The two patches are 280×280 and 160×160 pixels, respectively.

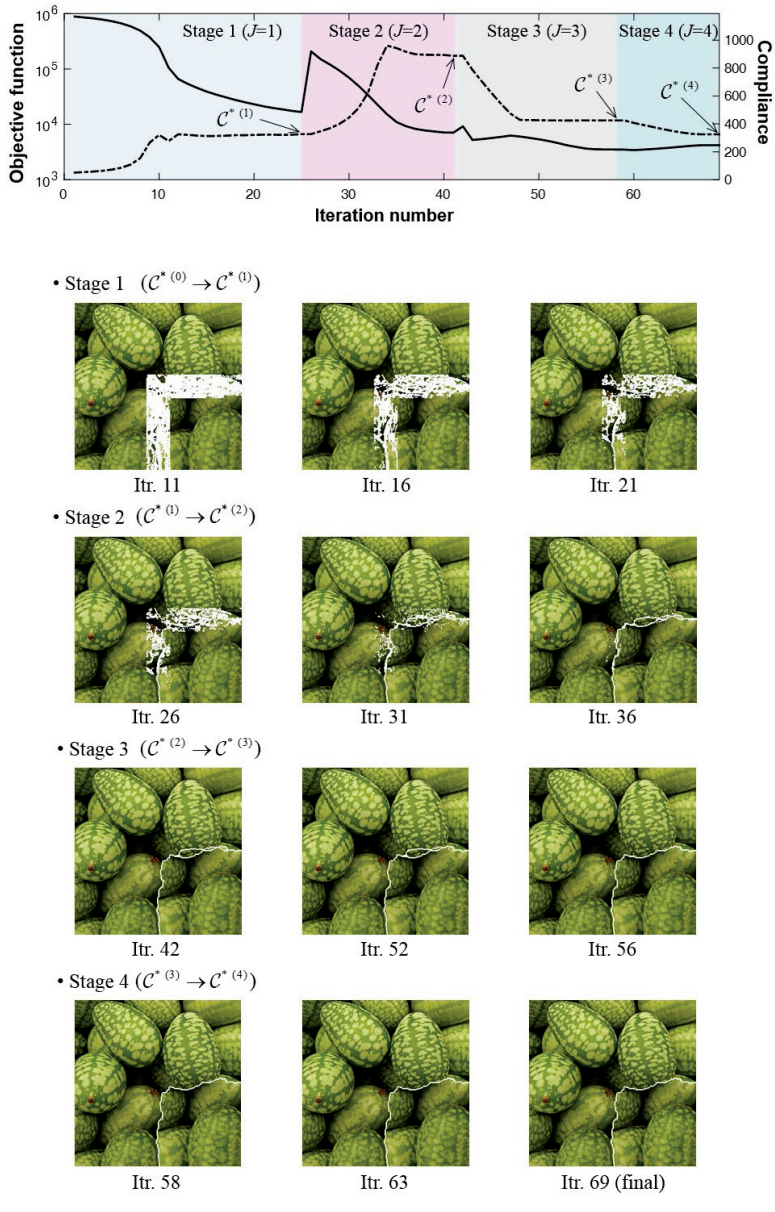

Figure 3.23 Iteration histories of the objective function (solid line) with compliance (dotted line) represented (top), and the evolution of the optimal heat path (i.e., seam) marked in white for images considered in Figure 3.15 (bottom).

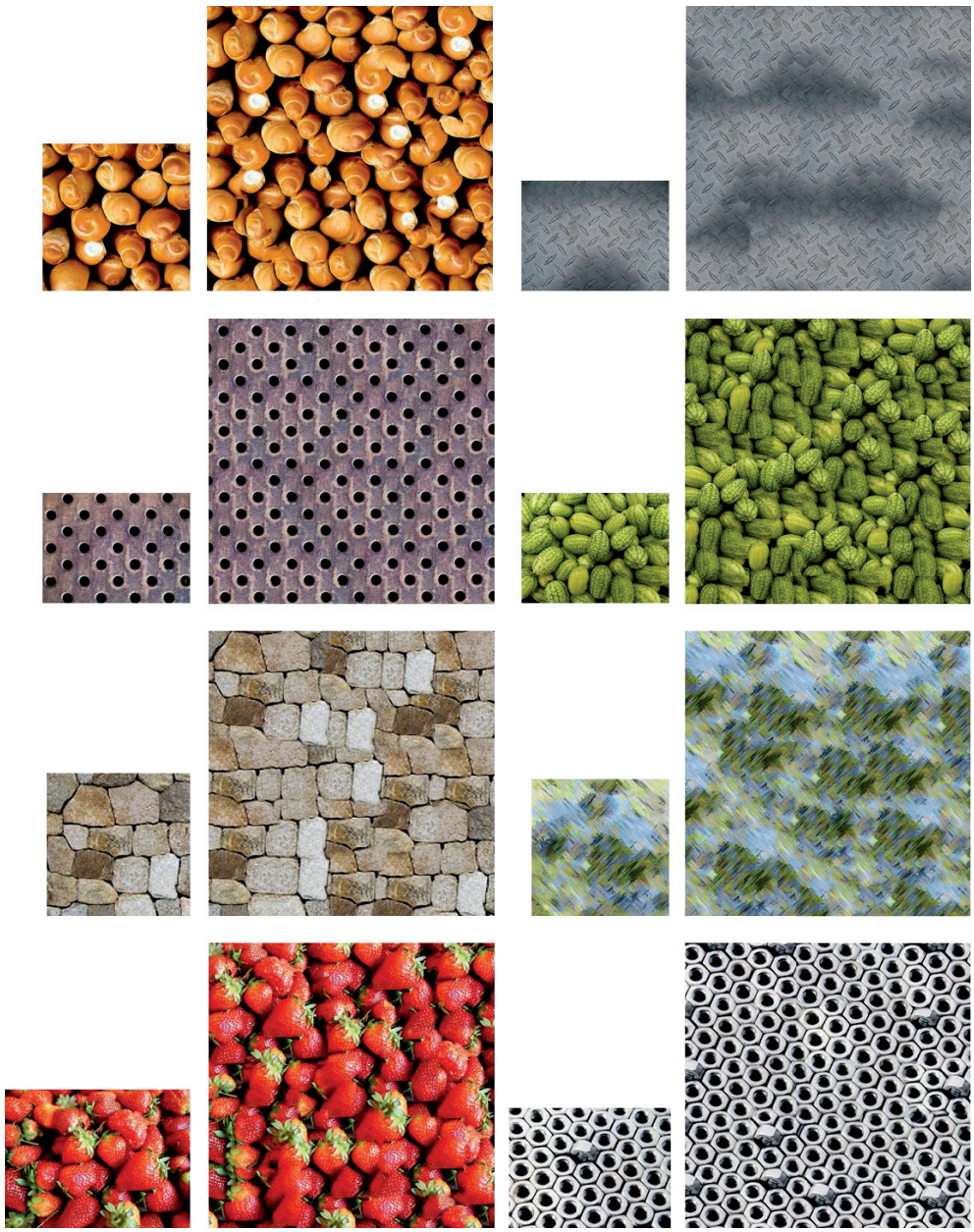

Figure 3.24 Results of texture synthesis for source images taken from © Flickr. The small images are source images and the large ones are those synthesized by the proposed algorithm.

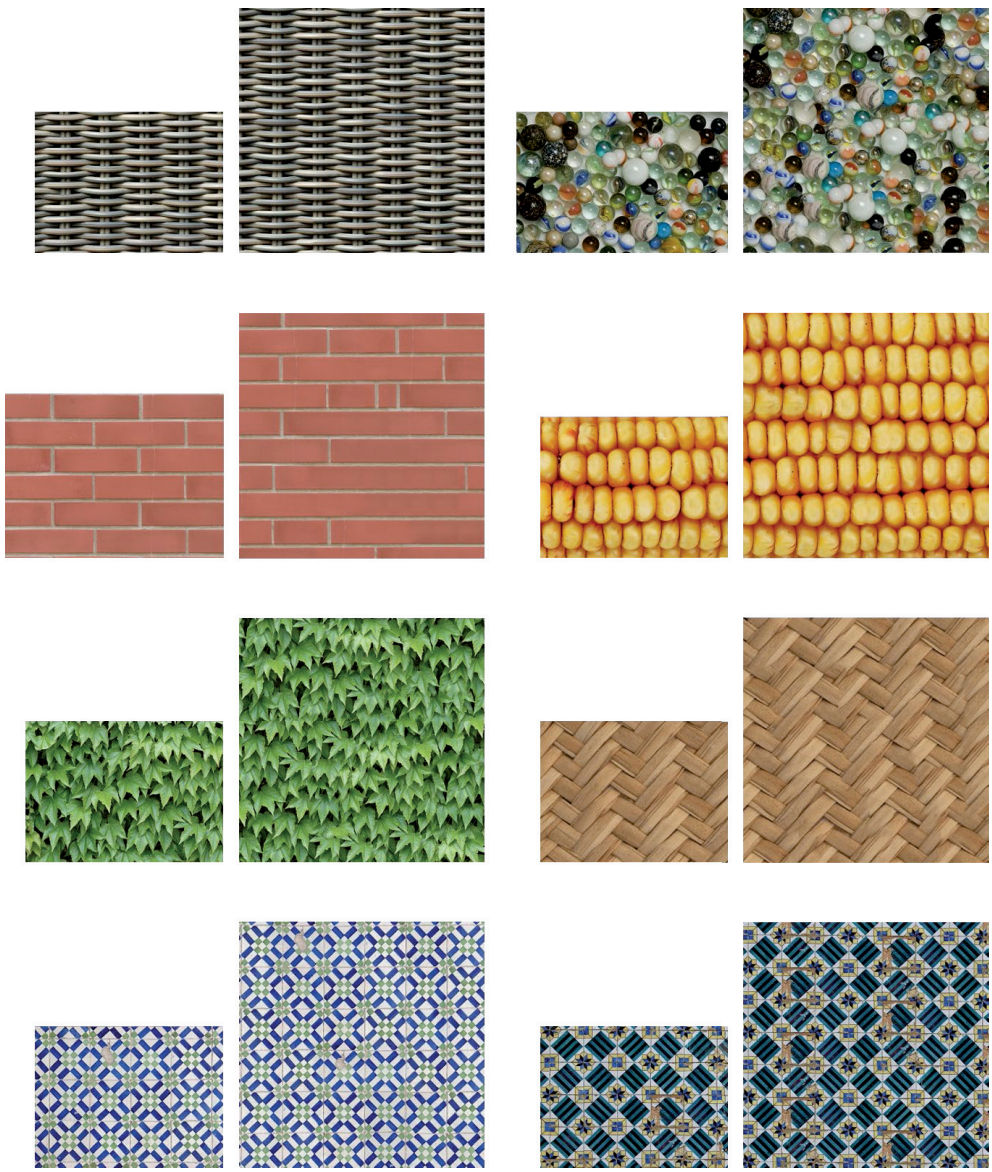

Figure 3.25 Results of texture synthesis for source images taken from © textures.com. The small images are source images and the large ones are those synthesized by the proposed algorithm.

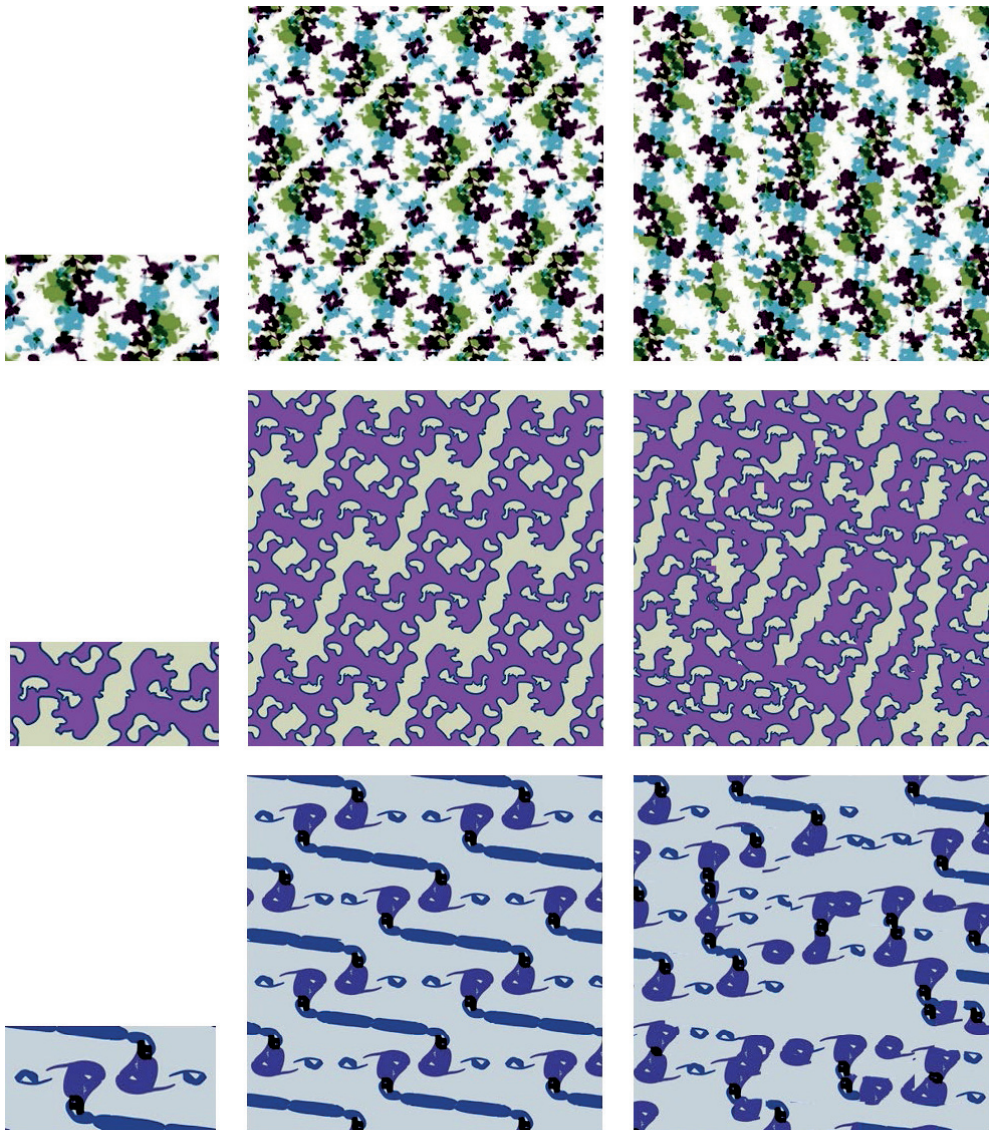

Figure 3.26 Results of texture synthesis for source images generated by the variational art algorithm (© Project33). The small images are source images and the large ones are those synthesized by the proposed algorithm.

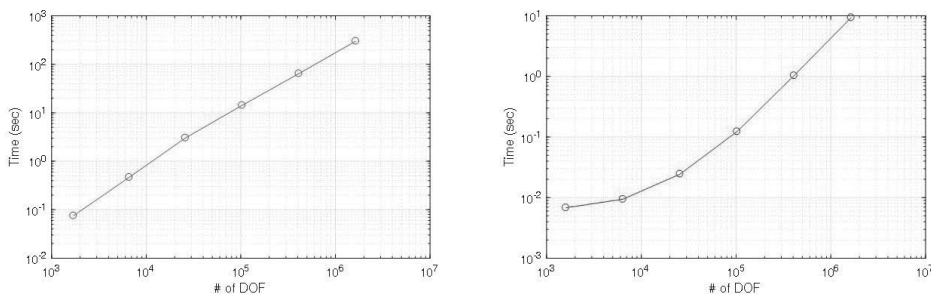

Figure 3.27 Comparison of the time complexity between (a) the proposed method based on topology optimization and (b) the graph-cut method based on max-flow algorithm.

CHAPTER 4
GENERATION OF PATTERN IMAGE AND ITS APPLICATION TO PRODUCT DESIGN

4.1 Overview

The Variational art (VA) algorithm, which is a research on creating new images through topology optimization for a heat transfer system, has been studied [16]. The image is created within the design domain where sources and sinks are randomly distributed by the optimization algorithm. In order to use various colors, the optimization process is performed the same number of times as the number of colors. In addition, the characteristics of the stroke of the image vary with the control of the parameters of the VA algorithm. The result images made by using VA can be artworks themselves. In order to make them more widely useful, we have tried to generate patterns from them. A pattern is an image in which motifs are repeated regularly. The

easiest way to generate a pattern is to simply reflect an image created by VA as a motif. This ensures that the boundaries of images are connected because the same borders are struck, but does not ensure the content of the image is naturally connected. This patterning scheme can only produce a limited pattern of characteristics. So, we have proposed the method of generating an image considering the pattern to be made of it in the process of creating an image, rather than merely reflecting it after creating an image. By making the content at the border of an image to continue when another image is placed next to it, a seamlessly connected pattern can be created. The previously study on the VA algorithm is briefly summarized in Section 4.1, the proposed method of creating images while considering connectivity at boundaries of images for pattern generation is explained in Section 4.2 and various prototypes on which patterns are printed are shown in Section 4.2.

4.2 Variational art algorithm

The VA algorithm that creates a single image (motif) already has been studied [16]. A part of generating a pattern image in this thesis is based on that algorithm. This section briefly summarizes the previous research on VA.

The VA algorithm is based on the topology optimization method to find efficient heat dissipating paths on a two-dimensional structure for a given set of heat sinks, sources and allowable mass usage. Only steady-state conduction and normal convection will be considered as in a research on the robot path planning. The governing differential equation for a temperature field θ distributed on a two-dimensional plate Ω is as follows

$$k\nabla^2\theta - h\theta + Q = 0 \tag{4.1}$$

The symbols k and h are the coefficients of thermal conductivity and convective heat transfer. Heat sources are denoted by Q. To solve the virtual problem to be used by the finite element method, the design domain where heat transfer takes place for given sources and sinks is discretized by two-dimensional finite elements (i.e., pixels or voxels). By following the standard finite element procedure, one can construct element-level stiffness matrix ($\mathbf{K}^e$) and nodal vectors (temperature $\boldsymbol{\theta}^e$ and load $\mathbf{F}^e$) and then form a system matrix equation

$$\mathbf{K}\boldsymbol{\theta} = \mathbf{F} \tag{4.2}$$

where $\mathbf{K}$, $\boldsymbol{\theta}$ and $\mathbf{F}$ denote the system-level counterparts. With these variables, the virtual design optimization problem is set up to minimize thermal compliance and subject to mass constraint as follows:

$$\underset{(\rho_1,\rho_2,\rho_3,\cdots,\rho_e)}{\text{minimize}} \ \Pi = \boldsymbol{\theta}^T \mathbf{K}\boldsymbol{\theta} \tag{4.3}$$

$$\text{subject to} \ \sum_{e=1}^{Ne} \rho_e V_e - M \le 0 \tag{4.4}$$

where ρ_e denotes the continuous density design variable allocated to every element and it represents the state of material presence in an element (0 for void and 1 for material presence) such that $0 < \rho_e \le 1$ ($e = 1, 2, \cdots, N_e$ (the number of elements)). The symbols M and V_e denote the allowed mass ratio in forming heat paths and the element volume, respectively. For the topology optimization setup, the element conductivity coefficient k^e needed in forming $\mathbf{K}$ is interpolated as a function of ρ_e. A polynomial interpolation of $k^e = k_e \rho_e^p$ is employed to express the element conductivity depending on material presence, where k_e is the nominal conductivity and p, the penalty exponent. To solve the topology optimization using a sensitivity-based optimizer such as the OC (optimality criterion) algorithm [1], the

sensitivity of the objective function Π with respect to ρ_e is calculated.

To use several colors in generating images, the following technique is proposed. The number of colors is defined as the number n_L of layers in the VA algorithm. For each layer, the topology optimization is solved separately by the formulation given above. After topology optimization problems are solved n_L times, the converged images obtained for n_L layers are then superimposed to make a final image. The color of each layer is represented by the triplet RGB color model $\mathbf{C}^l$ such that

$$\mathbf{C}^l = \left[r^l \ , g^l \ , b^l \right] \quad \left(l = 1, 2, \cdots, n_L \right) \tag{4.5}$$

where r^l, g^l and b^l take on integer values between 0 and 255. The color distribution $\mathbf{C}_e^l$ of the e^{th} finite element is conceptually proportional to the value of the element density design variable (ρ_e). This means that the brightness of the color $\mathbf{C}^l$ depends on the density value. Once $\mathbf{C}_e^l$ is determined for all elements for all color layers ($l = 1, \cdots, n_L$), the results can be superimposed, based on the subtractive color mixture for each layer.

There are many parameters used to define the virtual heat transfer system. First, the

effects of the distance between a heat source Ω_s and a sink Ω_E on generated images can be considered. Generally, the optimized path widens as the distance between the sink and the source decreases while it becomes slender as the distance increases. The effects of the numbers of heat sinks are similar to those of heat sources. The images obtained for a single source with a varying number of sinks and those for the reverse case are different even though the total number of sources and sinks are same. In addition, the total numbers of sinks N^E and sources N^S (with $N^E = N^S$) have an effect on the images. The more numbers of sink and source are used, the finer the obtained images are.

The parameters related to the topology optimization algorithm are also briefly covered. the penalty exponent p in the interpolation of the element conductivity coefficient $k^e = k_e \rho_e^p$ affects the resulting images. Distinct images are obtained for $p > 1$ while blurred images are obtained when $p = 1$. Although blurred images should be avoided in engineering applications, they can give an impression of ink-and-wash painting in images. In fact, the generation of such blurred images may be an advantage of the VA art algorithm. Also, distinct images appear as the iteration number j increases and the optimized path becomes thicker as the mass constraint ratio increase.

The VA algorithm can be also applied to a base image. In this case, the nominal

conductivity k_e may be set to be proportional to the brightness of the image at the corresponding element while the uniform value of $k_e = 1$ everywhere is assigned when no base image is used. In fact, the value of k_e controls how well the color is spread out spatially in the virtual system.

In previous study on VA, a method of reflecting an image was adopted to generate a pattern from an image made with VA. As shown in Figure 4.1, a unit image to be repeated for a pattern can be obtained by reflecting horizontally, vertically, horizontally and vertically.

4.3 Periodic boundary conditions for connectivity of motifs

Repeating an image means that one of the four boundaries of the image comes into contact with another boundary. In order for the image to be connected at boundaries, the pixels on both sides of the boundaries to meet should have the same RGB value. When the image is reflected with respect to the boundary as shown in Figure 4.1, the original image and the reflected one are easily connected because they share the identical boundary lines. There is a way to create a pattern by repeating an image so that different boundaries meet without reflecting it. We can consider two cases of repeating an image.

The first is the case where an image is repeated vertically and horizontally without reflection or rotation. In this case, the left and right boundaries and the top and bottom boundaries meet, respectively. These boundary conditions are similar to those used to design a unit cell of periodic elastic medium. In the design process of the heat transfer system, periodic conditions are applied to the nodal temperature $\boldsymbol{\theta}$ of the design domain not the design variable which is directly related to the RGB values of the pixel. The nodal temperature $\boldsymbol{\theta}$ of the design domain can be grouped as

$$\boldsymbol{\theta} = \left[\boldsymbol{\theta}_{in} \quad \boldsymbol{\theta}_{l} \quad \boldsymbol{\theta}_{u} \quad \boldsymbol{\theta}_{r} \quad \boldsymbol{\theta}_{b} \quad \boldsymbol{\theta}_{ul} \quad \boldsymbol{\theta}_{ur} \quad \boldsymbol{\theta}_{bl} \quad \boldsymbol{\theta}_{br}\right] \tag{4.6}$$

The subscripts denote the location of nodal points sequentially in accordance with *inner*, *left*, *upper*, *right*, *bottom*, *upper left*, *upper right*, *bottom left*, and *bottom right* of the design domain, respectively. By the periodic boundary condition for the first case mentioned above, $\boldsymbol{\theta}_r$ and $\boldsymbol{\theta}_b$ can be expressed in terms of $\boldsymbol{\theta}_l$ and $\boldsymbol{\theta}_u$, respectively. Similarly, $\boldsymbol{\theta}_{ur}$, $\boldsymbol{\theta}_{bl}$ and $\boldsymbol{\theta}_{br}$ can be expressed in terms of $\boldsymbol{\theta}_{ul}$. Therefore, the nodal temperature can be defined as $\boldsymbol{\theta}' = \begin{bmatrix} \boldsymbol{\theta}_{in} & \boldsymbol{\theta}_l & \boldsymbol{\theta}_u & \boldsymbol{\theta}_{ul} \end{bmatrix}$ by independent nodal temperatures.

The second is the case where the original image and the image rotated by 180 degrees are alternately repeated vertically and horizontally so that one boundary line is brought into contact with that line which is rotated by 180 degrees. For this condition, the nodal temperatures on all boundaries must be symmetrical with respect to the midpoints of boundary lines. Let's define the vectors of the nodal temperature of *left*, *upper*, *right*, *bottom* by dividing into two parts as

$$\begin{aligned} \boldsymbol{\theta}_l &= \begin{bmatrix} \boldsymbol{\theta}_{l,fw} & \boldsymbol{\theta}_{l,bw} \end{bmatrix} \\ \boldsymbol{\theta}_u &= \begin{bmatrix} \boldsymbol{\theta}_{u,fw} & \boldsymbol{\theta}_{u,bw} \end{bmatrix} \\ \boldsymbol{\theta}_r &= \begin{bmatrix} \boldsymbol{\theta}_{r,fw} & \boldsymbol{\theta}_{r,bw} \end{bmatrix} \\ \boldsymbol{\theta}_b &= \begin{bmatrix} \boldsymbol{\theta}_{b,fw} & \boldsymbol{\theta}_{b,bw} \end{bmatrix} \end{aligned} \tag{4.7}$$

The subscripts '*fw*' and '*bw*' denote the front part of the vector divided by half and

the other part of that, respectively. The reason for dividing each vector into two parts is the symmetry condition of four vectors in Equation (4.7). By the periodic boundary condition for the second case mentioned above, $\boldsymbol{\theta}_l$, $\boldsymbol{\theta}_u$, $\boldsymbol{\theta}_r$ and $\boldsymbol{\theta}_b$ can be expressed in terms of $\boldsymbol{\theta}_{l,fw}$, $\boldsymbol{\theta}_{u,fw}$, $\boldsymbol{\theta}_{r,fw}$ and , respectively. Therefore, the nodal temperature can be defined as $\boldsymbol{\theta}' = \begin{bmatrix} \boldsymbol{\theta}_{in} & \boldsymbol{\theta}_{l,fw} & \boldsymbol{\theta}_{u,fw} & \boldsymbol{\theta}_{r,fw} & \boldsymbol{\theta}_{b,fw} & \boldsymbol{\theta}_{ul} \end{bmatrix}$ by independent nodal temperatures. Then, $\boldsymbol{\theta}$ and $\boldsymbol{\theta}'$ are expressed by a transformation matrix $\mathbf{T}$ as follow

$$\mathbf{T}\boldsymbol{\theta}' = \boldsymbol{\theta} \tag{4.8}$$

Equation (4.2) is rewritten by substituting Equation (4.8) as

$$\mathbf{K}'\boldsymbol{\theta}' = \mathbf{F}' \tag{4.9}$$

where $\mathbf{K}' = \mathbf{T}^{\mathrm{T}}\mathbf{K}\mathbf{T}$ and $\mathbf{F}' = \mathbf{T}^{\mathrm{T}}\mathbf{F}$. In the finite element analysis during the topology optimization process, the image satisfying the continuous condition at boundaries of the image can be designed using Equation (4.9) instead of Equation (4.2). Figure 4.2 shows the motif generated with the boundary condition of the first case where an image is repeated vertically and horizontally without reflection or rotation, and the pattern which is made of the motif. Figure 4.3 shows the motif generated with the boundary condition of the second case where the original image

and the image rotated by 180 degrees are alternately repeated vertically and horizontally, and the pattern which is made of the motif. The two motif images were generated under the same initial conditions except for the boundary conditions. However, it can be seen that the motif images and the patterns made of them are quite different depending on applied boundary conditions. Figure 4.4 shows pattern images generated from motifs created under the same initial conditions except boundary conditions. Figure 4.4 (a) is a pattern obtained by reflection of the motif after it is created without any boundary conditions for continuity. Figure 4.4 (b) and (c) are the extended pattern of Figure 4.2 and 4.3. All the patterns in Figure 4.4 consist of 8×8 motifs.

4.4 Connectivity between different motifs

Section 4.3 deals with image generation that takes into account the connectivity of the motif and two cases for the translated or rotated motifs depending on how one motif which is created by VA with a single heat transfer condition is arranged. In this section, the connectivity of the image created by VA is considered for different heat transfer conditions. From the different heat transfer conditions, the two kinds of motifs made with the periodic boundary condition are connected well, respectively. But the two motifs are not connected naturally together. In order to connect different motifs, the connectivity between them should be considered in the process of creating motifs. When making a pattern with only one motif, the nodal temperatures for that are expressed as Equations (4.6) or (4.7) considering the connectivity of the motif depending on the ways of arrangement.

The method considering compatibility between adjacent microstructure has been studied for design of functionally graded materials [52]. Similarly, in order to secure the connectivity of two different motifs, a term that quantifies the degree of connectivity between them should be included in the objective function of the optimization for generating the motif. Most simple condition for connectivity between adjacent motifs is sharing elements across the interface. However, this condition does not reflect the characteristics of the heat transfer system. Therefore, we consider not only the interface of the motifs in the process of generating two motifs, but also the compound motif in which the two motifs are combined as shown

in Figure 4.5. The heat transfer characteristics of the compound motif can be used as a measure of the connectivity of the two motifs. The objective function is defined as a weighted sum of terms for each motif and the compounded motif. The objective function for topology optimization is expressed as follows.

$$\underset{\boldsymbol{\rho}}{\text{minimize}} \quad (1\text{-}w)(f(\boldsymbol{\rho}^A) + f(\boldsymbol{\rho}^B)) + w f(\boldsymbol{\rho}^{AB}) \tag{4.10}$$

$$\begin{aligned} \text{subject to} \; &: \sum_{e=1}^{N_A} \rho_e^A v_e^A - M^A \le 0 \\ &: \sum_{e=1}^{N_B} \rho_e^B v_e^B - M^B \le 0 \end{aligned} \tag{4.11}$$

where f is thermal compliance of individual or compound motifs, $\boldsymbol{\rho}^A$, $\boldsymbol{\rho}^B$ and $\boldsymbol{\rho}^{AB}$ are the design variable of motif A, B and compound motif and M^A and M^B are mass fractions for motif A and B. The symbol w is a weighting factor which determines the effect of the compound motif on design of the individual motifs. When w is 0, the individual motifs are designed without the connectivity between neighboring motifs, while w when is 1, each motif is designed with considering the connectivity between them in the compounded part as in Figure 4.7. The number and location of heat sources and sinks and mass fractions of two motifs are in Figure 4.6. When w is an intermediate value of 0.5, both motifs have a tendency to be smoothly connected themselves and to each other, but they are not perfectly connected. In order to improve the connectivity of designed motifs, the topology

optimization process considering the connectivity is additionally performed. Figure 4.8 shows this hierarchical motif generation process. To improve the connectivity in stage 2, these motifs designed in the previous stage are fixed and one or more motifs between them are newly generated in the same manner as in stage 1. In Figure 4.8, two motifs generated with $w = 0.5$ are the result of stage 1, and the interpolated motifs from them are the result of stage 2. Patterns with motifs obtained in stage 1 and stage 2 are shown in Figure 4.9. Two patterns look very similar, but the connectivity of motifs at the interface of stage 2 is slightly improved. In this way, as the number of stages of image creation increases, the connectivity of the motifs can be gradually improved. As a result, the connectivity of each individual motif and between each other are improved together, so that even if two different motifs are arbitrarily arranged, a seamlessly connected pattern can be created.

4.5 Application of patterns to the product design

We have created various motif images which are naturally connected at their boundaries when they are repeated to make pattern images by using the Equation (4.9) in the topology optimization process. Because a series of these works are performed by the algorithm on the computer, a large number of different pattern images can be generated by automated process. In addition, we collaborated with designers to commercialize a large amount of graphic images. Designers have selected and modified input images to be entered into the algorithm as well as refined graphic pattern images to the extent that they can be applied to the product. Through many discussions with designers, pattern images created by VA were applied to a variety of art works.

The first application is a pattern book about the theme of ‘Seoul National University’. In this work, several symbols related to 'Seoul National University' were used as input images. To generate a large number of different patterns, main parameters of VA such as the locations and the values of heat sources and heat sinks, parameters of the optimizer and color were randomly set in each image generation process. Through the analysis of the mass-produced images by the VA algorithm, the characteristics of the pattern images are defined. And pattern images can be classified into four categories according to the characteristics of the pattern: the strokes are thick and the input image is revealed well in the pattern, the strokes are thick and the input image is not revealed well in the pattern, the strokes are thin and

complex and the input image is revealed well in the pattern, the strokes are thin and complex and the input image is not revealed well in the pattern. Each category is subdivided into four subcategories (spring, summer, fall, winter). Figure 4.10 shows representative images of each category. A part of the pattern book that we made on the subject of 'Seoul National University' is shown in Figure 4.11. This pattern book contains not only a total of 400 patterns, but the product images to which the pattern is applied and parameter studies of the proposed algorithm.

The second application is the fabric products including ties, scarves, and clothing fabrics are selected. Generally, finely repetitive patterns are adopted for the tile and vivid and less repetitive patterns are adopted for the scarf. So the patterns which are obtained from the VA algorithm are simplified or sharpened depending on the characteristics of the product to be printed on. Prototypes of ties and scarves are shown in Figure 4.12. On the other hand, relatively large and fancy patterns are applied for apparel. Patterns for clothing are intentionally made fancy and complicated by combining two or more patterns. After patterns were digital-printed on fabrics such as silk or polyester, clothing prototypes were made of them after the ready-made garment by the tailor as shown in Figure 4.13.

The third application is an artwork. Patterns generated with the proposed algorithm can be artwork themselves due to their unique graphic characteristics. We created a variety of abstract patterns using symbol images such as corporate logos as input

images. This work was planned as a corporate promotional material with unique characteristics without directly revealing the logo. As part of the corporate promotional material, a picture that metaphorically represents the company's logo can be considered to be exhibited at important places like as in Figure 4.14. Pictures of patterns made in different repeating methods were produced as shown in Figure 4.15.

The VA algorithm for the pattern can generate a large number of patterns as shown in prototypes presented above, and the result images have unique characteristics which are very different from those intentionally made by the designer. In addition, the quality of the patterns made from the algorithm can be improved with the post-processing by the designer for applying to the actual product. Depending on the product to be applied, the color of the pattern image can be chosen diversly or simplified, or multiple patterns are synthesized in a flashy fashion. But only through these works of the post-processing the strict regularity of the pattern cannot be relieved because of repetitive motifs. Although regularaly repetitive patterns are used widely, a new approach to pattern generation is needed to create a more diverse and creative pattern. This is why the method of texture synthesis is introduced in Chapter 3.

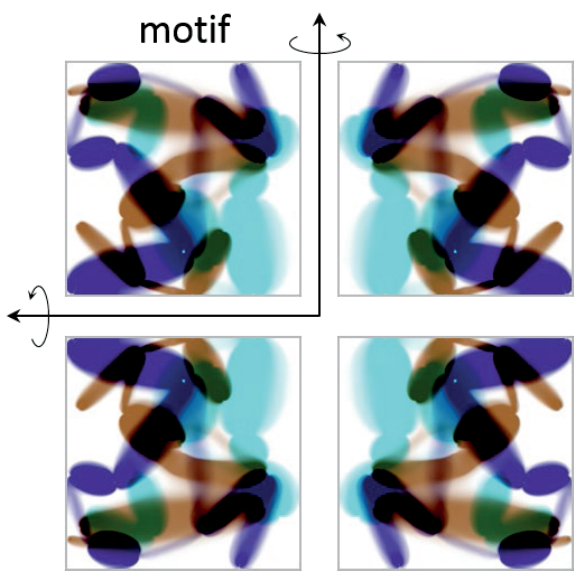

Figure 4.1 Reflection of the motif for a pattern generation.

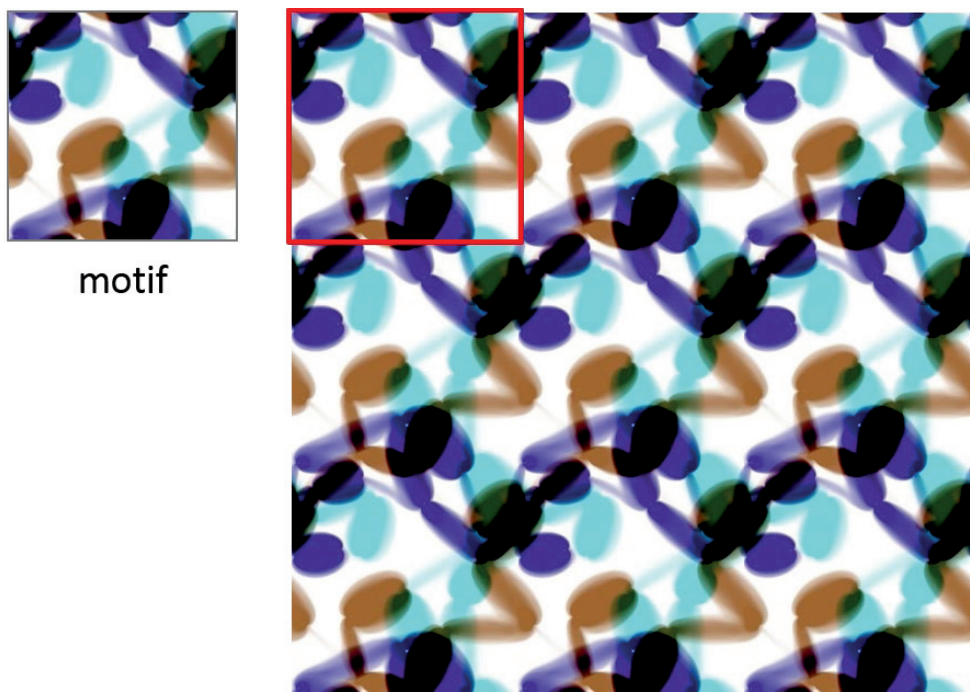

Figure 4.2 The motif created by using VA algorithm with the boundary condition where left and right boundaries and upper and lower boundaries match each other, and the pattern made by repeating the motif vertically and horizontally without reflection or rotation.

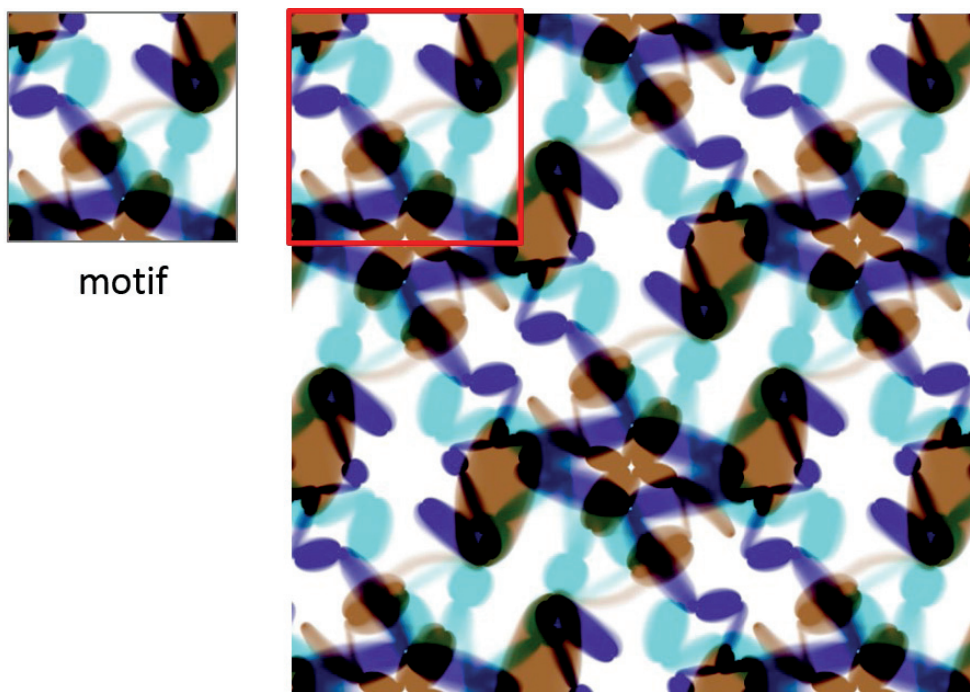

Figure 4.3 The motif created by using VA algorithm with the boundary condition where each boundary is symmetrical., and the pattern made by alternately repeating the motif and the rotated motif by 180 degrees vertically and horizontally.

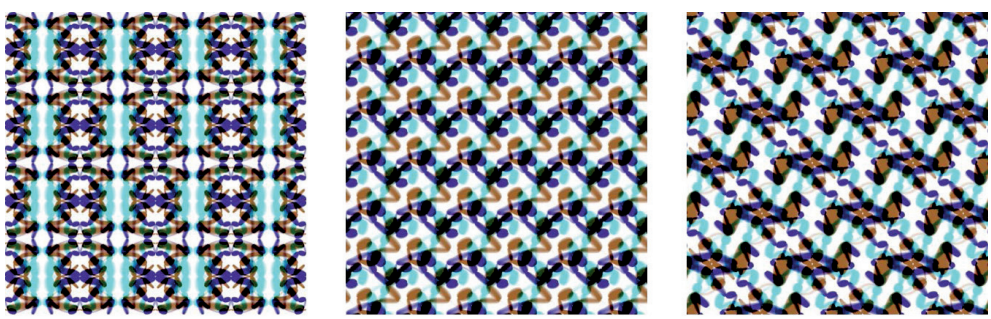

(a) (b) (c)

Figure 4.4 Patterns made by different ways: (a) reflecting the motif which is created without any boundary conditions for continuity, (b) repeating the motif vertically and horizontally without reflection or rotation and (c) repeating the motif and the rotated motif by 180 degrees alternately.

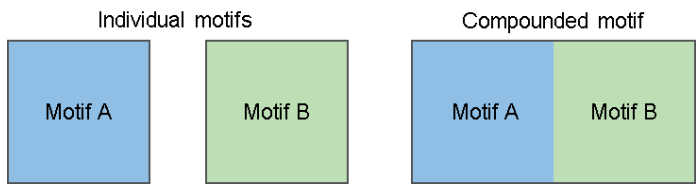

Figure 4.5 The concept of the compound motif composed of two individual motifs

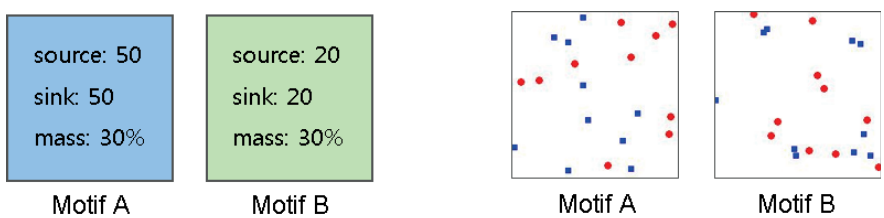

Figure 4.6 Conditions of heat transfer for generating motifs including the number and the location of heat sources and sinks and the volume fraction.

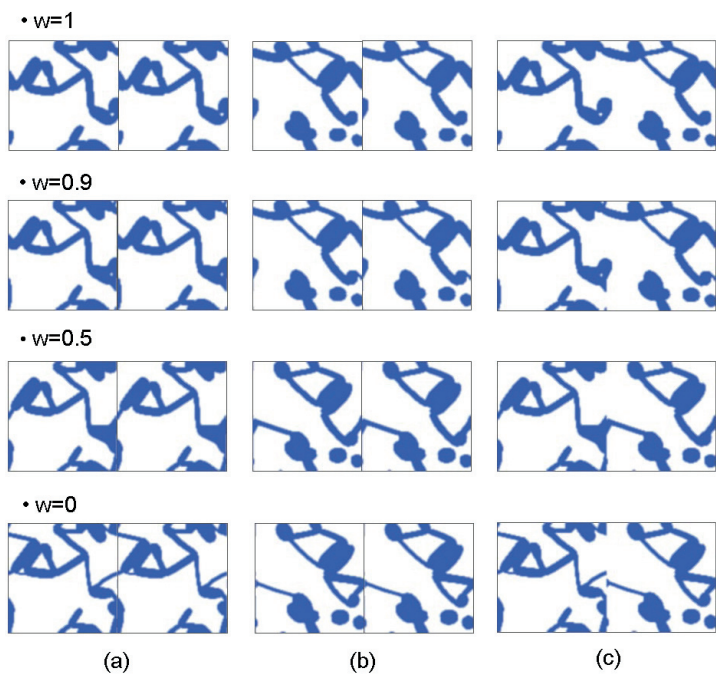

Figure 4.7 Motifs generated by VA algorithm considering the effect of compound motif. (a), (b) the repeated images of each individual motif, (c) the compound motif composed of two individual motifs.

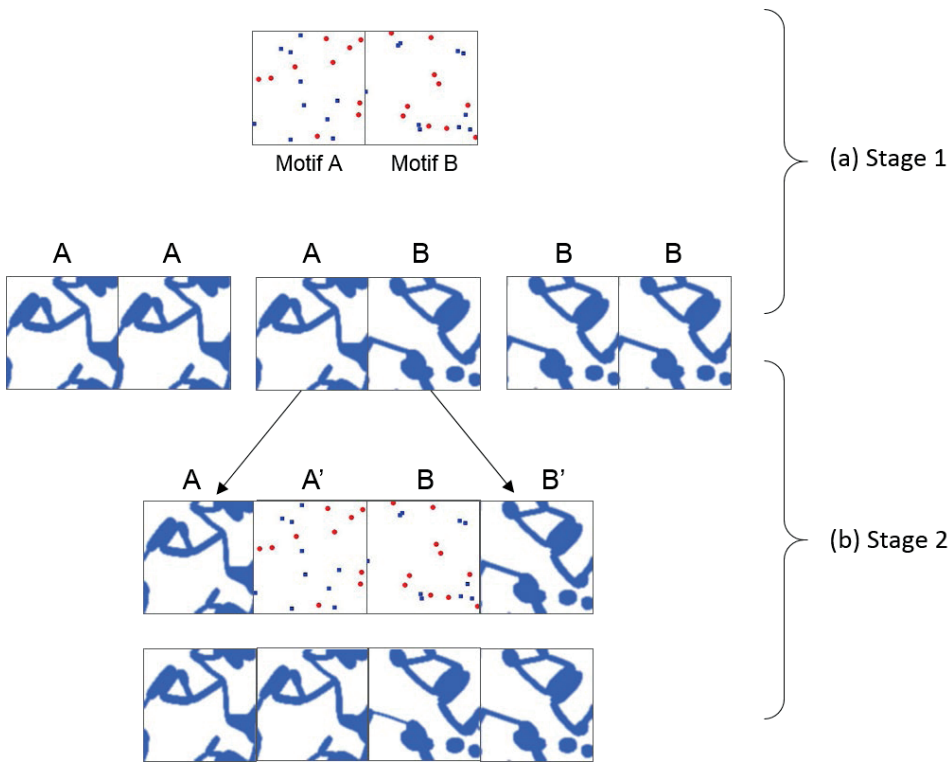

Figure 4.8 Interpolated motif generation scheme. (a) Stage 1: Individual motif A and B are generated through an optimization with considering the effect of the compound motif. (b) Stage 2: Intermediate motifs are generated with fixed motifs obtained at Stage 1

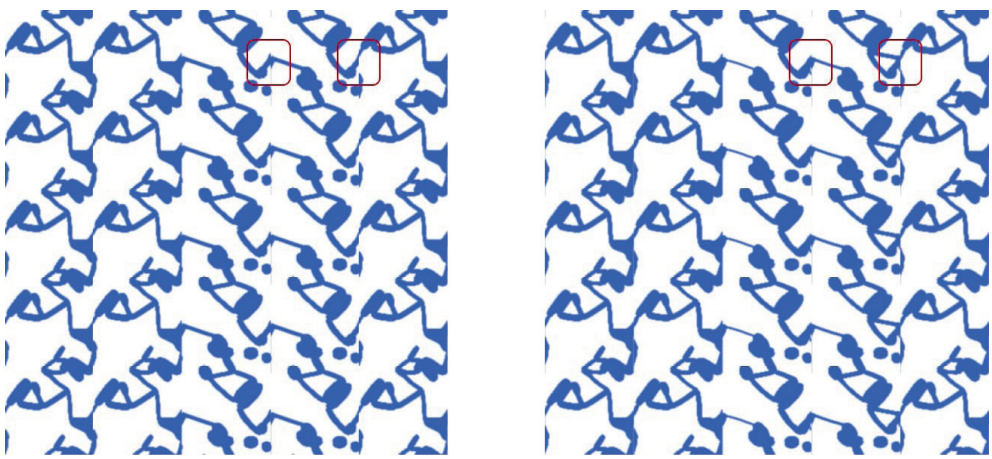

Figure 4.9 Patterns composed motifs obtained through (a) Stage 1 and (b) Stage 2.

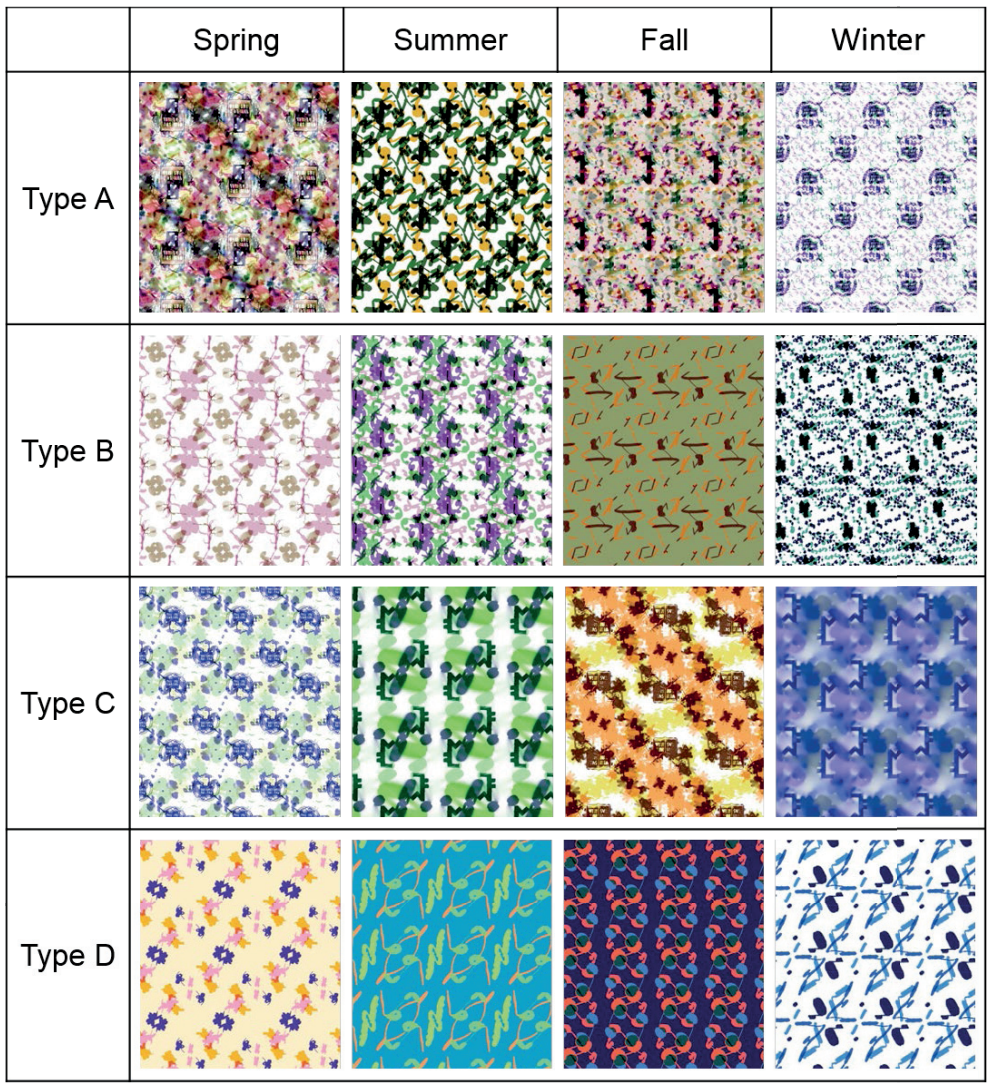

Figure 4.10 Representative images of each category in the pattern book on the theme of 'Seoul National University'.

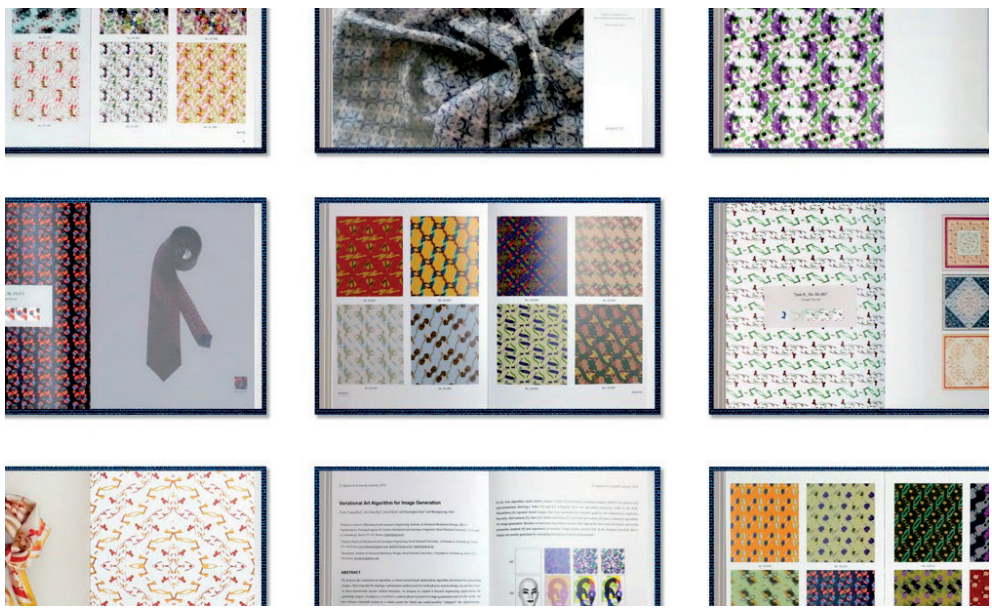

Figure 4.11 Various contents of the pattern book on the theme of 'Seoul National University'.

Figure 4.12 Sample products of ties and scarves with digital-printed patterns generated by using the proposed algorithm.

Figure 4.13 Sample products of clothing with digital-printed patterns generated by using the proposed algorithm.

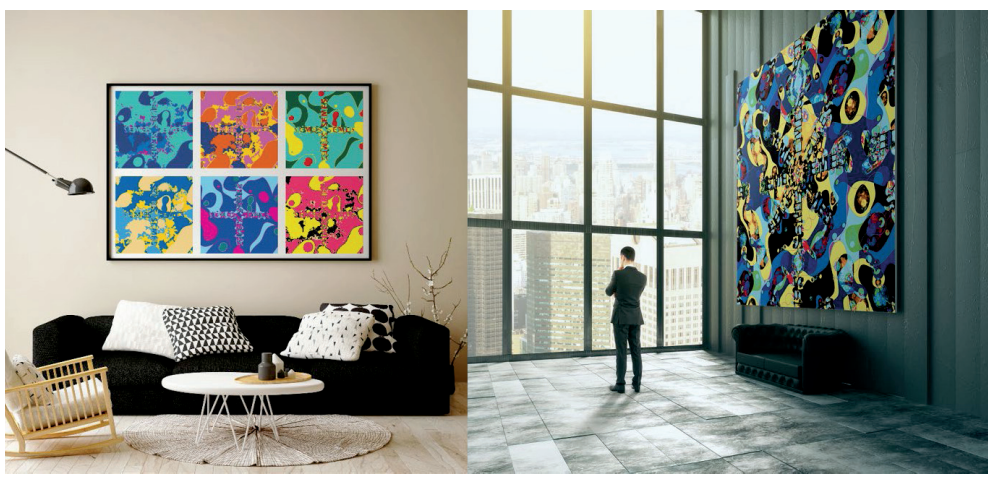

Figure 4.14 The concept of the art printing as a corporate promotion.

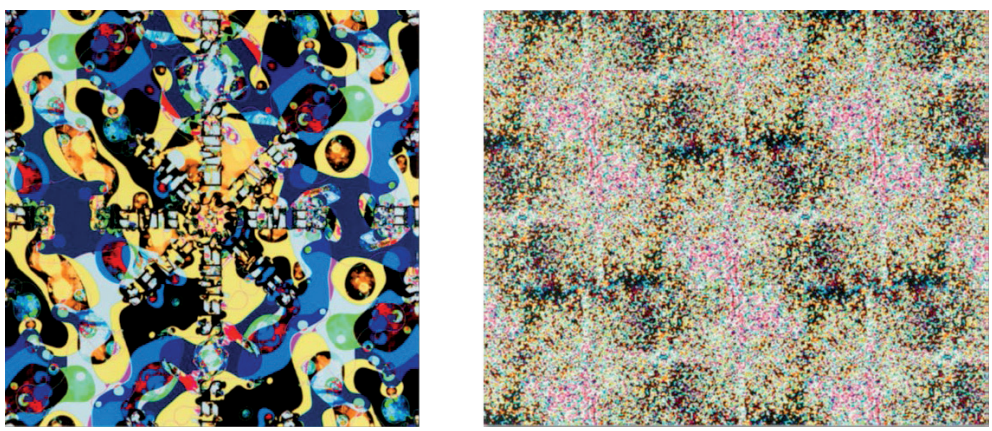

Figure 4.15 Sample products of the art printing made by printing patterns on canvas.

CHAPTER 5
CONCLUSIONS

In this thesis, graphic images with repetitive contents such as textures and patterns were designed by the sensitivity-based topology optimization of the heat transfer system. The topology optimization algorithm was used for finding a stitching seam to synthesize a texture and creating contents which compose a pattern image.

We solved the problem of texture synthesis by casting it into a form suitable approached by topology optimization in a simulated physical space. We solved the problem of finding an optimal seam to stitch patches, where this seam is compared to the optimal heat path connecting a heat source and a sink in a conducting plate-equivalently, the region of overlap of the patches to be stitched. Because of the comparison, the naturalness of patch connection comes from the physics of heat transfer. While techniques for the topology optimization of optimal heat paths are available, their direct applications to this problem result in only multi-line and/or

multiply connected heat paths that are not useful as stitching seams because they must be single line. To overcome this problem, we developed a double-loop topology optimization algorithm in which the inner loop solves minimization of the matching cost-weighted mass of the heat path under a constraint on thermal compliance, and the outer loop updates its constraint bound. The proposed method to estimate the bound can find the optimal solutions in simple validation problems. For most problems solved here, the typical number of executions of the outer loop was between three and four while the total number of iterations of topology optimization was no more than 100. Tests with more case studies of image synthesis confirmed that this double-loop algorithm is effective in generating single-line, natural-looking stitched patches. Because the proposed algorithm can be parallelized, we can solve even large problems efficiently if needed. Furthermore, the same algorithm can be directly extended to 3D problems, although this study focused on 2D problems. Moreover, this way of using topology optimization in the simulated physical space can be useful in various computer vision problems involving minimization.

For generating a repetitive pattern, the motif of the pattern was optimized by the VA algorithm based on topology optimization considering the connectivity of motifs. Depending on the way of the repetitive arrangement of the motifs, a completely different patterns can be generated from the motifs created under the same heat transfer conditions. The pattern created by the repetitive arrangement has regularity, which is a different characteristic from the texture created by image synthesis.

REFERENCES

[1] M. P. Bendsøe and O. Sigmund, Topology Optimization: Theory, Methods, and Applications. Springer Science & Business Media, 2003.

[2] M. P. Bendsoe and N. Kikuchi, Generating Optimal Topologies in Structural Design Using a Homogenization Method, Computer Methods in Applied Mechanics and Engineering, 71 (1988) 197-224.

[3] O. Sigmund and K. Maute, Topology optimization approaches, Structural and Multidisciplinary Optimization, 48 (2013) 1031–1055.

[4] S. I. Kim and Y. Y. Kim, Topology optimization of planar linkage mechanisms, International Journal for Numerical Methods in Engineering, 98 (2014) 265–286.

[5] J. S. Lee, E. I. Kim, Y. Y. Kim, J. S. Kim and Y. J. Kang, Optimal poroelastic layer sequencing for sound transmission loss maximization by topology optimization method, The Journal of the Acoustical Society of America, 122 (2007) 2097-2106.

[6] M. B. Dühring, J. S. Jensen and O. Sigmund, Acoustic design by topology optimization, Journal of sound and vibration, 317 (2008) 557-575.

[7] L. Lu, T. Yamamoto, M. Otomori, T. Yamada, K. Izui and S. Nishiwaki, Topology optimization of an acoustic metamaterial with negative bulk modulus using local resonance, Finite Elements in Analysis and Design, 72 (2013) 1-12.

[8] J. H. Oh, Y. K. Ahn and Y. Y. Kim, Maximization of operating frequency ranges of hyperbolic elastic metamaterials by topology optimization, Structural and Multidisciplinary Optimization, 52 (2015) 1023-1040.

[9] A. Iga, S. Nishiwaki, K. Izui and M. Yoshimura, Topology optimization for thermal conductors considering design-dependent effects, including heat conduction and convection, International Journal of Heat and Mass Transfer 52 (2009) 2721-2732.

[10] A. Gersborg-Hansen, M. P. Bendsøe and O. Sigmund, Topology optimization of heat conduction problems using the finite volume method, Structural and multidisciplinary optimization, 31 (2006) 251-259.

[11] T. E. Bruns, Topology optimization of convection-dominated, steady-state heat transfer problems, International Journal of Heat and Mass Transfer, 50 (2007) 2859-2873.

[12] J. Wu, C. Dick and R. Westermann, A system for high-resolution topology optimization, IEEE Transactions on Visualization and Computer Graphics, 22 (2016) 1195–1208.

[13] B. Zhu, M. Skouras, D. Chen, and W. Matusik, Two-scale topology optimization with microstructures, ACM Transactions on Graphics (TOG), 36 (2017) Article 164.

[14] J. Martínez, J. Dumas, S. Lefebvre, and L. Y. Wei, Structure and appearance optimization for controllable shape design, ACM Transactions on Graphics (TOG), 34 (2015) Article 229.

[15] J. C. Ryu, F. C. Park, and Y. Y. Kim, Mobile robot path planning algorithm by equivalent conduction heat flow topology optimization, Structural and Multidisciplinary Optimization, 45 (2012) 703-715.

[16] Y. Y. Kim, J. C. Ryu, E. Kim, H. Kim and B. Ahn, A variational art algorithm for image generation, Leonardo, 49 (2016) 226–231.

[17] Y. Kanno and X. Guo, A mixed integer programming for robust truss topology optimization with stress constraints, International Journal for Numerical Methods in Engineering, 83 (2010) 1675-1699.

[18] J. Smith, J. Hodgins, I. Oppenheim and A. Witkin, Creating models of truss structures with optimization, ACM Transactions on Graphics (TOG), 21 (2002) 295-301.

[19] W. Achtziger and M, Stolpe, Truss topology optimization with discrete design variables -guaranteed global optimality and benchmark examples, Structural and Multidisciplinary Optimization, 34 (2007) 1-20.

[20] M. Stolpe and A. Kawamoto, Design of planar articulated mechanisms using branch and bound, Mathematical programming, 103 (2005) 357-397.

[21] A. A. Efros and T. K. Leung, Texture synthesis by non-parametric sampling, In Proceedings of the 7th IEEE International Conference on Computer Vision, 1999, 1033–1038.

[22] L.-Y. Wei and M. Levoy, Fast texture synthesis using tree-structured vector quantization, In Proceedings of the 27th Annual Conference on Computer Graphics and Interactive Techniques. 2000, 479–488.

[23] V. Kwatra, A. Schodl, I. Essa, G. Turk, and A. Bobick, Graphcut textures: Image and video synthesis using graph cuts, ACM Transactions on Graphics (ToG), 22 (2003) 277–286.

[24] A. A. Efros and W. T. Freeman, Image quilting for texture synthesis and transfer, In Proceedings of the 28th Annual Conference on Computer Graphics and Interactive Techniques. 2001, 341–346.

[25] A. Lasram and S. Lefebvre, Parallel patch-based texture synthesis, In Proceedings of the Fourth ACM SIGGRAPH/ Eurographics conference on High-Performance Graphics, 2012, 115–124.

[26] M. Ashikhmin, Synthesizing natural textures, In Proceedings of the 2001 Symposium on Interactive 3D Graphics, 2001, 217–226.

[27] V. Kwatra, I. Essa, A. Bobick and N. Kwatra, Texture optimization for example-based synthesis, ACM Transactions on Graphics (ToG), 24 (2005) 795–802.

[28] A. Kaspar, B. Neubert, D. Lischinski, M. Pauly and J. Kopf, Self-tuning texture optimization, In Computer Graphics Forum, 34 (2015) 349–359.

[29] L. A. Gatys, A. S. Ecker, and M. Bethge, Texture synthesis using convolutional neural networks. In Advances in Neural Information Processing Systems, (2015) 262–270

[30] L. A. Gatys, A. S. Ecker, and M. Bethge, Image style transfer using convolutional neural networks. In Proceedings of IEEE Conference on Computer Vision and Pattern Recognition (2016), Article 161.

[31] O. Sendik and D. Cohen-Or, Deep correlations for texture synthesis, ACM Transactions on Graphics (ToG), 36 (2017)

[32] D. Ulyanov, V. Lebedev, A. Vedaldi and V. Lempitsky. Texture Networks: Feed-forward Synthesis of Textures and Stylized Images. Proceedings of the 33rd International Conference on Machine Learning (2016)

[33] C. Li and M. Wand 2016. Combining Markov random fields and convolutional neural networks for image synthesis. In Proceedings of IEEE Conference on Computer Vision and Pattern Recognition, 1 (2016) 2479-2486

[34] R. Verostko, Form, Grace and Stark Logic: 30 Years of Algorithmic Drawing, Leonardo, 43 (2010) 230–233.

[35] H. Cohen, A Self-Defining Game for One Player: On the Nature of Creativity and the Possibility of Creative Computer Programs, Leonardo, 35 (2002) 59-64.

[36] F. Nake, Computer art: a personal recollection, In Proceedings of the 5th conference on Creativity and cognition, 2005, 54-62.

[37] B. B. Mandelbrot, Fractals and an art for the sake of science, Leonardo, 22 (1989) 21-24.

[38] J. McCormack, Open problem in evolutionary music and art, Applications of Evolutionary Computing Lecture Notes in Computer Science, 3449 (2005) 428-436.

[39] K. Sims, Artificial evolution for computer graphics, Computer Graphics, 25 (1991) 319-328.

[40] E. Heijer and A. E. Eiben, Comparing aesthetic measures for evolutionary art, Applications of Evolutionary Computing Lecture Notes in Computer Science, 6025 (2010) 311-320.

[41] S. Todd and W. Latham, Evolutionary Art and Computers, London: Academic Press, 1992.

[42] A. Bastanfard and H. Mansourifar, A novel decorative islamic star pattern generation algorithm, In Proceedings of International Conference on Computational Science and Its Applications, 2010.

[43] R. Alexander, Mycelium, Available: http://onecm.com/projects/mycelium

[44] W. Baxter, J. Wendt, and M. C. Lin, IMPaSTo: A realistic, interactive model for paint, In Proceedings of the 3rd international symposium on Non-photorealistic animation and rendering, 2004, 45-56.

[45] J. Lu, C. Barnes, S. DiVerdi, and A. Finkelstein, RealBrush: Painting with examples of physical media, ACM Transactions on Graphics, 32 (2013) 117-128.

[46] N. Chu and C.-L. Tai, MoXi: Real-time ink dispersion in absorbent paper, In Proceeding of SIGGRAPH, 2005, 504-511.

[47] F. P. Incropera and D. P DeWitt, Fundamentals of heat and mass transfer, 5th ed. Wiley, New York, 2002

[48] T. J. R. Hughes, The finite element method: linear static and dynamic finite element analysis, Prentice Hall, 1987.

[49] K. J. Bathe, Finite element procedures, Prentice Hall, 1996.

[50] K. Svanberg, The method of moving asymptotes–A new method for structural optimization, International Journal of Numerical Methods in Engineering, 24 (1987) 359–373.

[51] Y. Boykov and V. Kolmogorov, An experimental comparison of min-cut/max-flow algorithms for energy minimization in vision, IEEE Transactions on pattern analysis and machine intelligence, 26 (2004)

[52] E. Garner, H. M. Kolken, C. C. Wang, A. A. Zadpoor and Jun Wu, Compatibility in microstructural optimization for additive manufacturing, Addictive manufacturing, 26 (2019) 65-75

ABSTRACT (KOREAN)

민감도 기반 위상최적화 알고리즘을 이용한 텍스쳐 합성 및 패턴 이미지 생성에 관한 연구

김 은 일
서울대학교 대학원
기계항공공학부

텍스쳐(texture)와 패턴(pattern)은 반복적인 컨텐츠(contents)로 구성되어 있는 그래픽 이미지를 말한다. 반복되는 컨텐츠인 모티프(motif)와 배열 방법에 따라서 이미지는 다양하게 생성될 수 있다. 본 논문에서는 민감도 기반(sensitivity-based)의 열전달 위상최적화(topology optimization) 알고리즘을 이용하여 작은 모티프로부터 독창적이고 다양한 텍스쳐와 패턴 이미지를 합성하는 방법을 다루었다. 텍스쳐나 패턴의 합성 과정에서 가장 중요한 것은 그것을 이루는 작은 이미지들이 끊김없이 자연스럽게 연결되는 것이다. 본 연구에서는 이와 관련하여 두 가지 방법을 제시한다. 첫 번째 방법으로, 컨텐츠가 반복되면서도 정형성(regularity)이 덜한 이미지를 생성하기 위해 컴퓨터 비젼(computer vision) 분야의 패치 기반 텍스쳐 합성(patch-based texture synthesis) 기술이

도입되었다. 여기서의 텍스쳐 합성이란 모티프로부터 유사한 컨텐츠의 패치들을 복사하여 그것들이 자연스럽게 연결되도록 꿰매는 작업이다. 합성된 이미지는 조금씩 다르면서도 유사한 컨텐츠의 패치들로 구성되므로 텍스쳐 또는 준정형적(semi-regular) 패턴이라고 할 수 있다. 패치를 연결하는 것에 있어서 가장 중요한 것은 꿰매기 위한 경로(stitching seam)를 찾는 것이다. 이를 위해서 기존의 컴퓨터 비젼에서 사용되는 알고리즘 대신 민감도 기반의 열전달 위상최적화 알고리즘이 새롭게 적용되었다. 특히 기존의 위상최적화에서 일반적으로 다루지 않는 단일 경로로의 수렴을 위해 주요 변수의 업데이트 과정이 포함된 이중 루프 알고리즘(double-loop algorithm) 이 고안되었다. 간단한 예제를 통해 제안하는 알고리즘의 타당성을 검증한 후 실제 텍스쳐 합성 문제에 적용하였고 경로의 수렴과 최적화 과정에서 이 방법의 유효성을 확인할 수 있었다. 또 다른 방법은 모티프 자체가 반복되어 정형적인 패턴을 이루는 경우, 모티프를 만들어내는 과정 중에 반복되는 모티프 사이의 연결성을 동시에 고려하는 것이다. 이렇게 설계된 모티프는 경계선에서 끊김없이 연결되어 동일한 모티프가 규칙적으로 배열된 패턴 이미지를 구성한다. 또한 모티브가 반복되는 배열 방향에 따라 다른 종류의 패턴이 합성될 수 있다. 우리는 제안한 방법으로 만든 패턴들을 일상 생활에서 쉽게 접할 수 있는 여러 제품군에 실제로 적용해보았다.

우리는 민감도 기반의 위상 최적화 알고리즘을 이용하여 다른 방식으로 정형화된 패턴과 준정형적인 텍스쳐 이미지를 성공적으로 만들어낼 수 있었으며, 제안하는 방법이 이미지를 생성하는 새로운 방법이 될 수 있음을 확인하였다.

주요어: 텍스쳐 합성, 패턴 제작, 민감도 기반 알고리즘, 위상최적화, 열전달 현상

학번: 2013-30193